(Re-)Imag(in)ing Price Trends*

Jingwen Jiang
Department of Computer Science
University of Chicago

Bryan Kelly
Yale University, AQR Capital Management, and NBER

Dacheng Xiu
Booth School of Business
University of Chicago

Abstract

We reconsider the idea of trend-based predictability using methods that flexibly *learn* price patterns that are most predictive of future returns, rather than testing hypothesized or pre-specified patterns (e.g., momentum and reversal). Our raw predictor data are images—stock-level price charts—from which we elicit the price patterns that best predict returns using machine learning image analysis methods. The predictive patterns we identify are largely distinct from trend signals commonly analyzed in the literature, give more accurate return predictions, translate into more profitable investment strategies, and are robust to a battery of specification variations. They also appear context-independent: Predictive patterns estimated at short time scales (e.g., daily data) give similarly strong predictions when applied at longer time scales (e.g., monthly), and patterns learned from US stocks predict equally well in international markets.

KEYWORDS: convolutional neural network (CNN), image classification, transfer learning, machine learning, technical analysis, return prediction

*We are grateful for comments from Ronen Israel, Serhiy Kozak (discussant), Ari Levine, Chris Neely (discussant), and seminar and conference participants at Washington University in St. Louis, University of Oxford, University of Rochester, Rutgers Business School, Boston University, Chinese University of Hong Kong, ITAM Business School, Singapore Management University, National University of Singapore, University of Science and Technology of China, SFS Cavalcade, Society of Financial Econometrics, China International Conference in Finance, Society of Quantitative Analysts, and INQUIRE UK. AQR Capital Management is a global investment management firm, which may or may not apply similar investment techniques or methods of analysis as described herein. The views expressed here are those of the authors and not necessarily those of AQR.

Nevertheless, technical analysis has survived through the years, perhaps because its visual mode of analysis is more conducive to human cognition, and because pattern recognition is one of the few repetitive activities for which computers do not have an absolute advantage (yet). Lo et al. (2000)

1 Introduction

A large literature investigates the ability of past prices to forecast future returns, producing a handful of famous and robust predictors including price momentum and reversal. The philosophical perspective underpinning these analyses is most commonly that of a hypothesis test. The researcher formulates a model of return prediction based on price trends—such as a regression of one-month-ahead returns on the average return over the previous twelve months—as a test of the weak-form efficient markets null hypothesis.

Despite some researcher's arguments otherwise, it is difficult to see in the literature a clearly articulated or theoretically motivated specific alternative hypothesis. Said differently, the price-based return predictors studied in the literature are by and large ad hoc and discovered through human-intensive statistical learning that has taken place behind the curtain of the academic research process.

In this paper, we reconsider the idea of price-based return predictability from a different philosophical perspective founded on machine learning. In particular, we emphasize that there is potentially much to learn about the behavior of price-based predictive patterns. Given recent strides in understanding how human behavior influences price patterns, it is reasonable to expect that prices contain subtle and complex patterns about which it is difficult to develop specific testable hypotheses. We devise an open-minded statistical learning approach to elicit the return predictive patterns that underly the data. This philosophy moves the research focus to tracing out the empirical landscape, and away from testing specific and often ad hoc alternative hypotheses, in the hope of gathering a more informed view of the data from which better theories and more pointed testable hypotheses may be developed.

Perhaps the most daunting challenge to the machine learning perspective on price-based return prediction is settling on a methodology to achieve a balance between two countervailing concerns. On one hand, we prefer a method that is flexible enough to find potentially complex predictive patterns. On the other hand, we prefer a method that is tractable and constrained enough so that we can interpret those patterns in order to inform future theory.[1] To negotiate this delicate tradeoff, we make two research design choices that together result in successful inference of new return-predictive patterns in past prices. First we represent historical prices

[1] In addition to interpretability, we also favor more tractable and constrained methods to ensure that they can be reliably estimated from available data with manageable computational cost.

as an image, and second we model the predictive association between images and future returns using a convolutional neural network (CNN). These are conjugate choices that work together and enhance each other. We describe the logic behind each choice in turn, beginning with the CNN.

The input to a CNN is typically an image, and in our setting the image is a plot of past market information (open, high, low, and close prices and trading volume) represented as a 2D matrix. A CNN is designed to produce forecasts from an image without requiring the researcher to first decide how to convert the image into predictive features. Instead, the CNN automates the feature extraction process. In a given "layer" the CNN spatially smooths image contents to reduce noise and accentuate shape configurations that correlate with future returns. This smoothing operation is applied recursively by stacking multiple layers together, which gives the CNN its flexibility for capturing a vast range of predictive patterns (and earns it the synonym "deep learning"). In the last layer, the numeric pixel values from each position in the smoothed image become the final predictor set. At a high level, this is similar to more traditional kernel-based data filters used in regression analysis. But the CNN does not simply fix the set of smoothing filters. It instead estimates the filters that best detect shapes and other attributes of the images that are most predictive of the target variable. In short, we use a CNN due to its ability to automatically extract predictive signals from raw input data, which makes it ideally suited to elicit patterns that underly financial markets but that are likely too complex to be hypothesized based on existing theories.

Our research design embeds 1D time series data in a *higher* dimensional space, representing it as a 2D image, before bringing it to predictive analysis. Why is it beneficial to encode market data as an image rather than directly modeling the 1D data with a time series model? The first reason is that the leading CNN architectures are custom crafted for image analysis. Therefore, to enjoy the CNN's benefits of automated signal generation, it is useful to represent price data in the format naturally ingested by the CNN, i.e. as an image. Second, representing time series as an image allows the model to focus on relational attributes of the data that would be difficult to tease out with time series methods. It is the same basic logic for why humans illustrate patterns graphically rather than with lists of numbers. If a human can more readily detect patterns in images by consuming an entire data matrix through a single visualization, a statistical pattern recognition algorithm may benefit from it as well. Third, the process of imaging price and volume data converts all assets' data histories to a comparable scale. We show that this particular re-scaling choice has large benefits for prediction in the panel of stocks.

Our empirical analysis revolves around a panel prediction model for US stock returns from

1993 to 2019. We train a panel CNN model to predict the direction (up or down) of future stock returns. That is, in each training sample, we estimate a single model with a fixed structure and set of parameters that produces forecasts for all individual stocks. The data input to this model are images depicting price and volume (daily open, close, high, and low prices, daily trading volume, and moving average price) over the past 5, 20, and 60 days. The output of the CNN is a set of stock-level estimates for the probability of a positive subsequent return over short (5-day), medium (20-day), and long (60-day) horizons. We use CNN-based out-of-sample predictions as signals in a number of asset pricing analyses.

Our main empirical finding is that image-based CNN predictions are powerful and robust predictors of future returns. The CNN achieves out-of-sample classification accuracy (predicting positive versus negative subsequent returns) with an accuracy in excess of 53% for one month returns. This is a statistically significant improvement over the accuracy implied by standard technical signals such as momentum and short-term reversal. We provide a heuristic calculation to illustrate how seemingly small gains in forecast accuracy, of even 1% to 2% like we find using the CNN, can translate into large performance gains for trading strategies based on these predictions.[2]

Next, we show directly how the CNN model's forecasts translate into out-of-sample portfolio performance. We sort stocks into decile portfolios using image-based CNN forecasts and track the returns of a decile spread H-L portfolio. We first consider a monthly return strategy. Image-based decile spreads perform extraordinarily well, earning annualized out-of-sample Sharpe ratios as high as 2.4 for equal-weight portfolios and 0.5 for value-weight portfolios. We benchmark this performance against three simple strategies: 2-12 momentum (MOM), 1-month short-term reversal (STR), and 1-week short-term reversal (WSTR). Of these, the closest competitor to image based forecasts is WSTR, which achieves Sharpe ratios of 1.2 and 0.3 in equal weight and value weight spread portfolios, respectively. The performance differential between the CNN and WSTR does not appear attributable to differences in limits to arbitrage such as trading costs. Image-based CNN strategies have portfolio turnover that is nearly identical to WSTR, but manage to double the annualized performance of WSTR.

We find similar qualitative results for strategies with longer holding periods of one quarter. The image-based H-L strategy reaches an annualized out-of-sample Sharpe ratio of 1.3 and 0.5 in equal weight and value weight terms, respectively. At a shorter holding period of one week, the distance between image-based CNN predictions and alternative signals grows. Equal weight strategies that rebalance weekly earn annualized Sharpe ratios as high as 7.2 (1.5 for value weight strategies). Rather than interpreting these results as trading results that are

[2]We derive a classification accuracy analogue to the translation from predictive R^2 into Sharpe ratio improvements proposed by Campbell and Thompson (2008).

achievable in practice, the one week strategy is meant to demonstrate the impressive predictive strength of images at short horizons relative to a well-understood benchmark while being interpretable in economic terms. We also show that this short-horizon predictive power can translate into long range predictability via transfer learning. Given such strong performance of image-based signals at the one week horizon, we show that the CNN also outperforms MOM and STR over monthly and longer horizons even if we *exclude* the first week of post-formation returns. In some cases, image-based strategies continue to earn a Sharpe ratio of 0.9 for one-month holding periods when trading is artificially delayed by a week beyond the end of the sample represented in the input image.

An intriguing aspect of our analysis is that return-predictive patterns detected by the CNN extrapolate to contexts outside of the main data set of daily US stock prices. In particular, we consider the possibility of image-based *transfer learning*, using a model estimated in one context to forecast in a distinct context. We show that the predictive patterns identified by the CNN from daily US stock data transfer well to international markets and to other time scales.

The most constraining aspect of empirical asset pricing data is in the time series dimension. The finance literature focuses most often on monthly data because the most economically important patterns in asset markets unfold over monthly or lower frequencies. Yet we experience only one history of financial market prices, meaning that we have at most several hundred monthly time series observations and several dozen annual observations. Given the scarcity of low frequency data, it would be greatly beneficial to know if patterns that unfold at high frequencies (which we can potentially measure well thanks to the availability of large high frequency data sets) are similar to patterns that unfold at low frequencies. Mandelbrot's (2013) hypothesis of "self-similarity" (also "scaling" or "fractal" behavior) in financial markets predicts that asset prices exhibit statistically similar patterns when studied at different time scales, and also predicts the emergence of long-range dependence in prices (Cont, 2005).

Transfer learning provides a means of investigating the possibility that price patterns apply at multiple time scales. While it is difficult, if not impossible, to effectively train a CNN using monthly, quarterly, or annual data, we can apply our CNNs trained on daily data to data sampled at lower frequencies. To illustrate this idea, we take a CNN model trained to predict 5-day ahead returns from images of 5-day prior market data and transfer it to the problem of predicting data sampled at lower frequencies. For example, if we reinterpret the 5-day CNN as a "5-period" model, with each period corresponding to a 12-day interval, then our 5-day CNN model can be applied to images of 60-day market histories sampled once every twelve days, and the resulting forecasts can be interpreted as forecasts of future 60-day returns. We

show that a quarterly holding period H-L strategy based on this approach delivers an out-of-sample annualized equal weight Sharpe ratio of 0.9. For comparison, a CNN trained directly on 60-day images to forecast 60-day returns earns an equal-weight Sharpe ratio of 0.4.

We also study the possibility of international CNN transfer. International markets have fewer stocks and shorter time series compared to the US. If estimates from the US are applicable in international contexts, it helps alleviate the limitations of conducting data-intensive analysis in small markets. More generally, if predictive patterns in stock prices are to some degree global phenomena, then forecasts in data sparse markets can draw estimation strength from information in data rich markets. We test the viability of international transfer by using CNN model estimates from US data to construct return forecasts in 26 foreign markets. We compare transfer-based H-L strategies in each country to a strategy based on a CNN estimated from scratch using local data. We find that transfer learning boosts the Sharpe ratio of country-level H-L strategies (with one month holding period) by 0.4 on average, from 0.3 with a locally-trained CNN, to 0.7 when directly applying the same CNN trained on US data.

We attempt to interpret the predictive patterns identified by the CNN. The ideal interpretation would answer the question "what does the CNN see when making its predictions?" CNN interpretation is a notoriously difficult problem in the machine learning literature because the model uses several telescoping layers of non-linear image transformations to generate its forecasts. We consider a variety of approaches to make progress on the interpretation challenge. First, we compare image-based signals from the CNN to previously studied signals in the literature. Via logistic regression, we identify the linear combination of signals that most closely approximates the CNN's prediction. We find that the obvious candidates, including a variety of price trend signals, measures of liquidity, and measures of risk, explain only 12% or less of the cross-sectional variation in CNN forecasts. Among these, image-based signals share the strongest correlations with dollar volume, size, reversal, and Amihud illiquidity.

Second, we search for a linear regression of the data underlying images that best approximates the CNN model. We find that a key component of image-based prediction accuracy is the implicit data scaling achieved by the image representation. In particular, images put all stocks' past price data on the same scale so that their recent maximum high and minimum low prices span the height of the image and rescale all other prices (open, high, low, close, and moving average) accordingly, and likewise for volume. In doing so, the model is able to more effectively compare and contrast images to make powerful cross-sectional inferences regarding future directional price moves. Following this data transformation, a linear model can produce a reasonable approximation to the CNN which aids in interpretation. For example, the linear approximation shows that when a stock closes on the low end of its recent high-low

range, future returns tend to be high. This is a simple and robust approximator for one of the patterns detected by the CNN. Yet the full non-linear CNN formulation generally improves on the linear approximation.

Third, we use CNN visualization methods from the machine learning literature to understand how different image examples "activate" different regions of the CNN model to eventually trigger an "up" or "down" return prediction. At last, as in the machine learning literature more broadly, our attempts at interpretation are admittedly incomplete. Yet they achieve partial success by offering some visibility into the complex inner workings of the CNN model.

A large literature has debated the theoretical sensibility and empirical reliability of technical analysis. Lo et al. (2000) and Lo and Hasanhodzic (2010) insightfully juxtapose arguments on either side of the debate. A number of papers present theoretical arguments for the existence of equilibrium predictability with technical analysis, including Brown and Jennings (1989), Grundy and McNichols (1989), Blume et al. (1994), Barberis et al. (1998), and Han et al. (2016), among others. Several papers find strong empirical support for technical trading rules, with prominent examples including Brock et al. (1992), Lo et al. (2000), Zhu and Zhou (2009), Neely et al. (2014), and Detzel et al. (2020). Sullivan et al. (1999) and Bajgrowicz and Scaillet (2012) study large collections of candidate trading rules with careful corrections for multiple hypothesis testing and reach skeptical conclusions regarding the significance of technical trading profits. The debate about the viability of technical trading is to some extent moot given the widely documented, robust, and by now uncontroversial momentum effect (Jegadeesh and Titman, 1993), which Schwert (2003) concludes is the most reliable technical pattern in the post-publication sample.

We contribute to this literature with an investigation of price trends (and technical analysis more generally) by presenting an exhaustive machine learning analysis. The key differentiator of our approach is that we do not require the researcher to pre-specify a set of technical patterns. Instead, we simply present our model with historical market data in the form of an image. In place of human-generated predictive signals, our CNN conducts an automated search for image patterns that are most predictive of future returns. One may view this as a continuation of the agenda set forth by Lo et al. (2000), but with a re-tooled research design benefitting from twenty years of progress in machine learning and computer vision. In the end, our CNN model extracts powerful and robust reliable predictive patterns from images that outperform stalwart price trend patterns from the literature, including momentum and short-term reversal.

Lastly, there is an emergent literature in computer science that uses price plots and CNN-

based models to forecast stock returns. These papers give a short description of methods and present small-scale empirical analyses. The large majority of this work performs time series prediction of aggregate stock indices (examples include Chen et al., 2016, Kim and Kim, 2019, Lee et al., 2019, Hoseinzade and Haratizadeh, 2019) who study time series prediction of aggregate stock indices. Hu et al. (2018) use price plot CNN's to cluster individual stocks, but do not predict returns. To our knowledge, no other paper performs a large-scale, thorough, and methodologically transparent analysis of return prediction for individual stocks with the fine granularity that is standard in empirical asset pricing research.

The remainder of the paper proceeds as follows. First, we describe the process of "imaging" market data in Section 2. Section 3 presents the intuition and detailed mechanics of our CNN framework. We report our main empirical analysis in Section 4. In Section 5, we analyze the benefits of CNN transfer learning across geographies and time scales. Section 6 explores interpretations of the CNN model, and Section 7 concludes. We report a variety of extensions and robustness of our main empirical analysis in the appendix, along with simulation evidence to illustrate the model's finite sample properties.

2 "Imaging" Market Data

In this section, we describe the process of representing historical market data as an image input for the CNN prediction model. Many popular websites such as Bloomberg, Yahoo! Finance, and Google Finance provide historical price charts for a wide range of financial assets. Figure 1 illustrates an example of Tesla's stock price data through August 18, 2020 in a common price chart format. It includes "OHLC" bars that depict daily opening, high, low, and closing prices. It then overlays a 20-day moving average closing price. The bottom of the chart shows daily trading volume. While these charts (and many variations on them) can be captured from the Internet, we instead generate our own price charts from scratch. This allows us to conduct various experiments by controlling the amount of information that our CNN "trader" can observe.

2.1 The OHLC Chart

The images we generate follow the basic format of Figure 1. In particular, our main price plot uses OHLC bars as illustrated in Figure 2a. High and low prices are represented by the top and bottom of the middle vertical bar, while opening and closing prices are represented by the small horizontal lines on the left and right of the bar, respectively. In our images, one day occupies an area three pixels wide (the center bar, open mark, and closing mark are each one pixel wide). We opt for OHLC rather than a candlestick chart (also commonly used to depict prices, see Figure 2b) because OHLC uses fewer pixels to convey the same information.

Figure 1: Tesla OHLC Chart from Yahoo! Finance

Note: OHLC chart for Tesla stock with 20-day moving average price line and daily volume bars. Daily data from January 1, 2020 to August 18, 2020.

The main component of our image is a concatenation of daily OHLC bars over consecutive 5, 20, or 60-day intervals (approximately weekly, monthly, and quarterly price trajectories, respectively). The width of a n-day image is thus $3n$ pixels. We replace prices by CRSP adjusted returns to translate the opening, closing, high and low prices into relative scales that abstract from price effects of stock splits and dividend issuance.

Once days are concatenated, we impose a constant height for all images and scale the vertical axis so that the maximum and minimum of the OHLC path coincides with the top and bottom of the image. As a result, all images for the same number of days have the same pixel dimensions. The resulting image is shown in Figure 3a.

The vertical dimension of the image conveys two main types of information. The first and most obvious are directional price trends that are viewed as the critical content of typical technical signals such as momentum and reversal. The second and more subtle is volatility information. Parkinson (1980) shows that the daily high-low range, described by the vertical length of the OHLC bar, provides an accurate snapshot of daily stock price volatility. Generalizations by Dobrev (2007) and others show that the high-low range over intervals other than a day are likewise beneficial for volatility inference. This helps motivate the visual representation of price paths, which allows the viewer to immediately and simultaneously perceive price ranges at different frequencies, which is an essentially non-linear process. This type of non-linearity would be difficult for traditional kernel methods to discern from time series data.

Figure 2: Comparison Between the OHLC chart and the Candlestick Chart

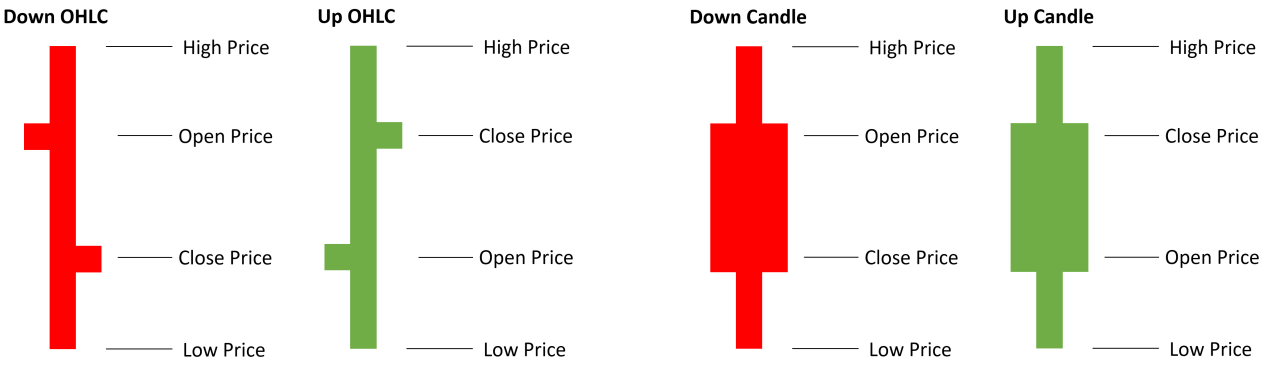

(a) OHLC chart (b) Candlestick chart

We exclude images for stocks that IPO or delist during the data window, but we allow missing data if it occurs in the middle of the stock's history. If there is missing data, the columns of pixels corresponding to the missing days are left blank (or partially blank if only part of the OHLC information is available).[3]

We use black as the background color and white color for visible objects on the charts. This means that most space on the chart is in black, which eases data storage requirements because a black pixel is represented by $(0, 0, 0)$ and our resulting images are sparse. The use of different colors for "up" and "down" days, as commonly used by Bloomberg and others, is redundant because the direction of price change is implied from the opening and closing price marks. This allows us to focus on 2D pixel matrices, rather than having to track a third dimension for RGB pixel intensities.

2.2 Moving Average Lines and Volume Bars

As in the Yahoo! Finance chart of Figure 1, we consider supplementing the main OHLC image with two additional pieces of information. The first is a moving average price line. In traditional technical analysis, moving averages are viewed as useful for inferring potential deviations from fair value by providing a long horizon reference point for prevailing point-in-time prices. The comparison of price to its moving average may be useful as a value signal that avoids the need for balance sheet data, as recommended by Fama and French (1988) and Kelly and Pruitt (2013). We use a moving average line with a window length equal to the number of days in the image (e.g., 20-day images will have a moving average line of 20 days). The daily moving average is reported using one pixel in the middle column for each day, and

[3]The ability to obtain price-trend based forecasts in the presence of incomplete data is an example of image-based CNN robustness to noisy data. When a high or low return is missing, we leave the bar entirely black because it is impossible to draw the middle bar. If both high and low prices are available but opening and closing prices are not, we draw a vertical bar only.

Figure 3: Examples of 20-day Image under Different Settings

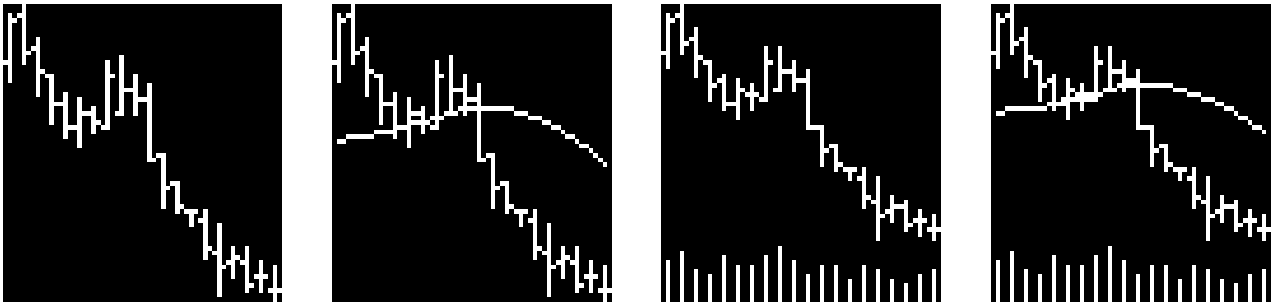

(a) w/o VB, w/o MA (b) w/o VB, w/ MA (c) w/ VB, w/o MA (d) w/ VB, w/ MA

Note: From left to right are 20-day images (a) without volume bar and moving average line, (b) without volume bar but with moving average line, (c) with volume bar but without moving average line, and (d) with volume bar and moving average line.

Table 1: Image Dimensions of the OHLC Chart with/without Volume Bars

	Sample Size (in Days)	Image Width (in Pixels)	Image Height (in Pixels)	
OHLC	5	15	32	
	20	60	64	
	60	180	96	
			Prices	Volume Bars
OHLC+V	5	15	25	6
	20	60	51	12
	60	180	76	19

a line is drawn by connecting those dots. See Figure 3b for an example of 20-day image with a moving average line added.

The second addition is a set of daily trading volume bars. When including volume data, we design images so that volume is shown in the bottom one-fifth of the image while the top four-fifths contain the main OHLC plot. Similar to our OHLC scaling, the maximum volume in a given image is set equal to the upper limit of the volume bar section and the remaining volume bars are scaled accordingly. See Figure 3c for an example 20-day image with volume bars added, and Figure 3d for an example with all price, moving average, and volume elements. In order to assess the predictive contribution of these elements, the appendix reports prediction sensitivity analyses using OHLC charts with and without moving average and volume elements according to the four combinations in Figure 3. Table 1 summarizes pixel dimensions for each of the design choices we consider.

Figure 4 shows examples from our final image data set. These images concisely embed a variety of information on price trends, volatility, intraday and overnight return patterns,

Figure 4: Generated OHLC Images with Volume Bar and Moving Average Line

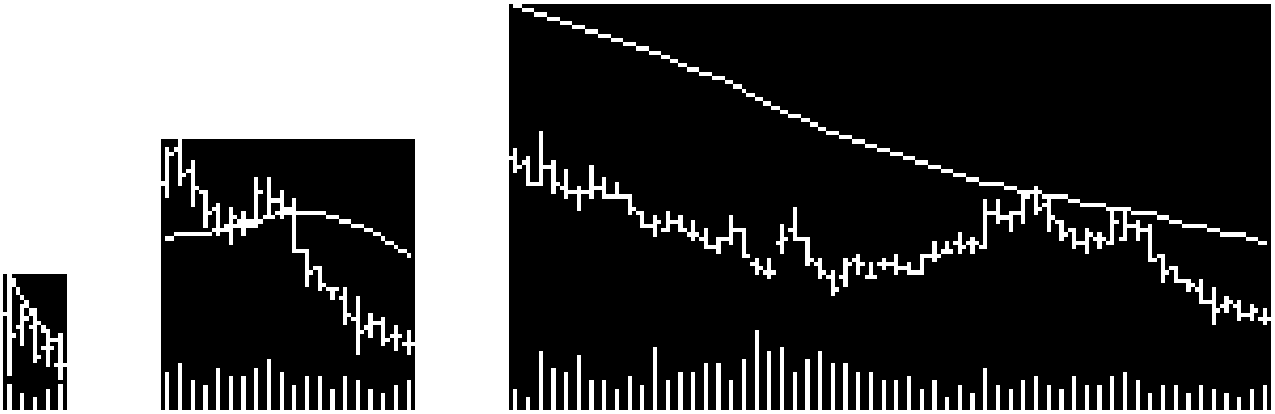

(a) 5 (b) 20 (c) 60

Note: Market data images for 5, 20, and 60 days of data.

and trading volume. The image design strikes a balance between information content and storage efficiency, delivering a rich information set as an input to the CNN while controlling the computational burden of estimation.

3 The Convolutional Neural Network Model

In this section, we describe the architecture of our CNN model. We present the model in detail and provide intuition for each of its components.[4] This section is admittedly dense, a necessity to provide interested researchers with a fully transparent understanding of model structure. Readers interested in the empirical results that do not desire an in-depth model treatment are encouraged to skip to Section 4. Once a description of the architecture is in place, we use it to discuss the rationale and beneficial aspects of raising the dimensionality of market data series from 1D time series to 2D images for use in a 2D CNN, rather than using a traditional time series prediction model.

Each image in our dataset is represented as a matrix of pixel values (0 or 255 for black or white pixels). In principal, this matrix can be vectorized and treated as the input to a standard feed-forward neural network. There are a number of problems with this approach. First, generic unconstrained neural networks tend to be massively parameterized, and this problem is exacerbated by the large number of pixels in a typical image. The amount of data required to support such a flexible parameterization is unrealistic in many research problems, and particularly in our application. Second, such a model would be inherently sensitive to position, scale, and orientation of an object in the image. Moving the object from one corner

[4] Goodfellow et al. (2016) Chapter 9 provides a textbook introduction to CNN.

of the image to another, or from foreground to the distance, would in general confuse such a model and severely limit its usefulness in forecasting.

Instead, CNN is the workhorse model for constructing predictions based on raw image data. Its popularity stems from its success in resolving the two problems above. They impose cross-parameter restrictions that dramatically reduce parameterization relative to standard feed-forward neural networks, making them more tractable to train and effective in prediction with comparatively small data sets. And they embed a number of tools that make the model resilient to deformation and re-positioning of important objects in the image.

3.1 Architecture of the CNN

A CNN is a modeling scheme that stacks together a sequence of operations to transform a raw image into a set of predictive features and, ultimately, a prediction. They are inherently modular, using a single core building block that can be assembled in various configurations depending on the application at hand. A core building block consists of three operations: convolution, activation, and pooling.

The first operation in a CNN building block is "convolution." To understand convolution, consider the simpler operation of applying a kernel smoother to a 1D time series. For example, a rectangular kernel with a width of three smooths the time series by scanning through observations, averaging each data point with its two neighbors. Convolution works similarly by scanning through the image and, for each element in the image matrix, producing a summary of image contents in the immediately surrounding area.

More specifically, the convolution operation uses a set of "filters." A filter is a low dimension kernel weighting matrix that, for each matrix element in the image, calculates the weighted average of the immediately adjacent matrix elements. Figure 5a is an illustrative example with a 6×6 image that is white in the 4×4 upper-left corner and black elsewhere. Filter 1 is an example of a 3×3 filter taking the values of $(1, 0, -1)$ in each row. For each interior element (i, j) of the image, the convolution operation sums the element-wise product of Filter 1 and the 3×3 image contents centered on (i, j). The result is stored in the corresponding element of the convolution output matrix.[5]

The example highlights the critical difference between convolution and 2D kernel smoothing. Smoothing calculates local averages in the image matrix, while convolution instead calculates a weighted sum of nearby image contents where the filter weights are parameters to be estimated. Through estimation, the CNN constructs filters that emphasize aspects of im-

[5]For elements at the image's border, we fill in the absent neighbor elements with zeros in order to compute the convolution. This is a common CNN practice known as "padding," and ensures that the convolution output has the same dimension as the image itself (see Simonyan and Zisserman, 2015).

Figure 5: Illustration of Convolution and Max-pooling Operations

(a) Illustration of a Convolutional Operation

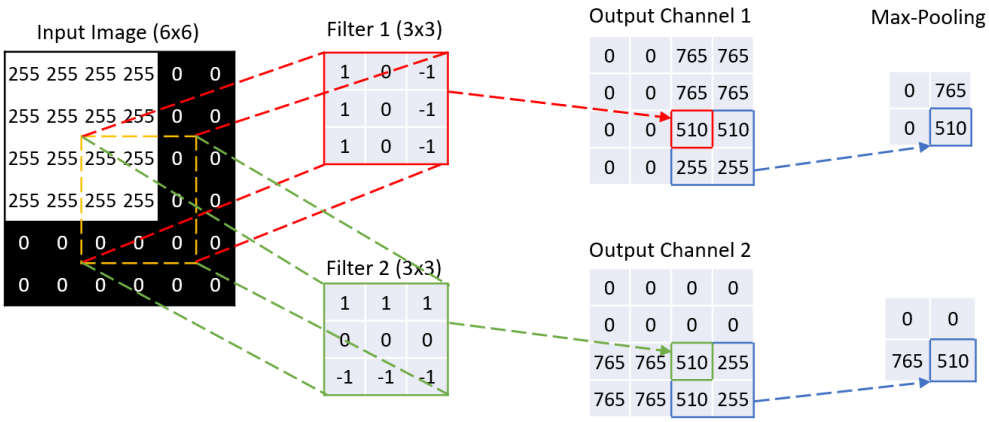

Note: The input tensor has size 6×6 (with only one channel of grey-scale). There are two 3×3 filters that detects edges. By construction, Filter 1 detects vertical edges and Filter 2 detects horizontal edge. When Filter 1 is applied to the yellow part of the input, the convolutional operation first calculates the element-wise products between the 3×3 yellow tensor and Filter 1 of the same size (solid red line) and then sums up the products and output a scalar (dotted red arrow) to the corresponding output location. As we can see from Output Channel 1, the right part of the output is activated by large values while the left part remains inactivated with all zeros, indicating that there is a vertical line on the right of the input image. Finally, the 2×2 max-pooling is applied to the output and shrinks the shape by half from 4×4 to 2×2 by taking the max out of the 2×2 rolling window from the output. The final output in channel 1 has value 765 at the upper-right corner and value 510 at the bottom-right corner, represented the extracted information that there are vertical edges on the right and the vertical edge is sharper at the top than at the bottom. Filter 2 is applied in the same sense (green dotted line and green dotted arrow) to extract the information that there are horizontal edges at the bottom of the image and the bottom-left (765) has sharper change than the bottom-right (510).

(b) Robustness to Noise from Max-Pooling

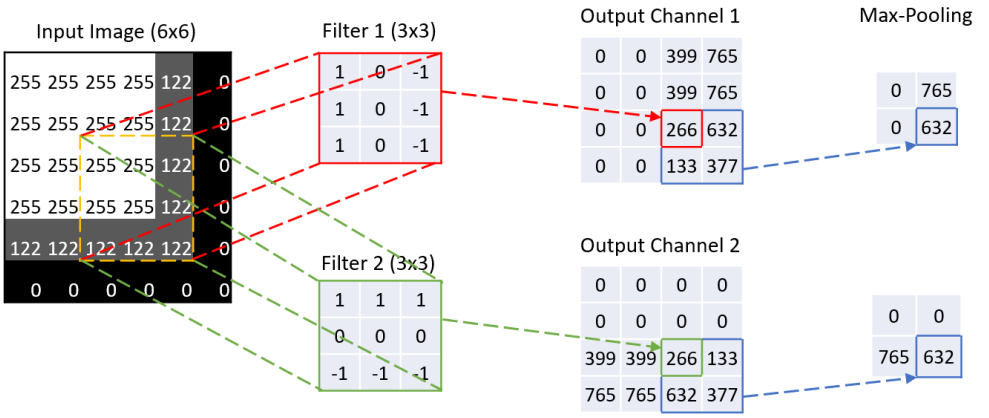

Note: This example shows that the introduction of the max-pooling layer adds robustness to noise. We take the same 6×6 image from the above example and blur the borderline with grey color (pixel value 122). Take Filter 1, which detects vertical edges, for example. Non-zero values from Output Channel 1 are significantly changed. However, after max-pooling is applied, the original upper-right value 765 remains intact while the original bottom-right value 510 is replaced with 632, a slightly larger number, indicating a slightly stronger signal of vertical line at the bottom than before. We observe a similar effect for Filter 2, which detects horizontal edges.

ages that are most predictive of the outcome of interest and blurs out uninformative content. The weight configuration in Filter 1, for example, is particularly useful for detecting vertical boundaries, while Filter 2 finds horizontal boundaries. Sliding the filter over the entire image amounts to searching the image for this specific pattern. If such a pattern exists in part of the input image, the corresponding output value will be large—meaning that the output neuron is stimulated and signaling that a pattern is detected. As in our model below, it is common to use several filters in a CNN, each specializing in certain patterns and thus each outputting a different set of features for use in the next layer of the model. And it is common for a CNN to use telescoping layers of filters, with the output from the filters in one layer of the CNN used as inputs for the subsequent layer to capture more complex patterns.

We use a filter size of 5×3 pixels in our baseline model. In addition, a convolution is flexible in "stride" of the filter, which defines the number of horizontal or vertical steps the filter takes as it moves through the image matrix. A larger stride corresponds to coarser convolution output. We use horizontal stride of one and vertical stride of three, meaning that the filter slides across the image and recalculates the filter output at every position in the row and jumps three rows at a time as it moves down the image vertically. We sometimes use a "dilated" filter to cover a larger neighborhood on the image than the size of the filter. A dilated filter with a dilation rate k along the vertical or the horizontal dimension (or both), expands the size of the original filter by filling in $(k-1)$ zeros in between adjacent entries along the corresponding dimension(s). Our baseline model uses a vertical dilation of two and no horizontal dilation.[6]

Convolution endows the CNN with a number of attractive properties relative to more general neural networks connecting an $N \times M$ input matrix to an $N \times M$ output. The CNN tightly constrains model parameterization by imposing two forms of (severe) cross-parameter restrictions. First, CNN applies a small filter uniformly to all locations in an image, while a general network allows separate weight parameters for each element of the image matrix. Second, the CNN maps the information from a given location in the input matrix *only* to the neighborhood of the same location in the output matrix, while a general network would allow for cross-connectivity between all elements of the input and output matrices. These restrictions, known respectively as "parameter sharing" and "sparse interactions," are critical to the tractability and small-sample robustness of the CNN. And, because the same filters are applied uniformly to all locations in the image, they detect relevant objects regardless of their

[6]Unit stride is a common choice in the CNN literature, but larger strides are sometimes used to reduce the dimensionality of the model. A stride of two, for example, recalculates the convolution at every other element of the input matrix, giving coarser convolution output with half the dimensionality. While both stride and dilation reduce the computational burden and encourage parsimony, dilation preserves the resolution of the original image.

position (in other words, CNN forecasts are "translation equivariant").

The second operation in a building block is "activation." This simple operation is a non-linear transformation applied element-wise to the output of a convolution filter. The activation function we use is "leaky ReLU." This, roughly speaking, takes the max of the filter output value and zero, which sharpens the resolution of the convolution filter output.[7]

The final operation in a building block is "max-pooling." We implement this operation using a small filter that scans over the input matrix and returns the maximum value the elements entering the filter at each location in the image. The role of max-pooling is two-fold. First, it acts as a dimension reduction device. Nearby neurons output from the convolution operation often carry similar information. If any of the neurons in the filter region are stimulated, max-pooling detects it. At the same time, it discards locally redundant information. For example, a 2×2 pooling filter shrinks the height and width of the input by half, and does so without introducing new parameters to be estimated further promoting parsimony in the CNN. In this respect, max-pooling is an image counterpart to the familiar idea of down-sampling from the signal processing literature. Second, by taking local maxima throughout the image, the output is left generally unaffected by small perturbations of the input pattern (illustrated in Figure 5b). In this sense, max-pooling is a de-noising tool that enhances CNN robustness to local deformation, much like the convolution operation aids CNN robustness to variation in object position.

Figure 6 illustrates how convolution, activation, and max-pooling combine to form the basic building block for a CNN model. These blocks are then stacked together to customize predictive CNN models with varying degrees of richness. In general, the data input to a building block is a tensor with dimensions $h \times w \times d$. The lingua franca of CNN refers to image depth d as the number of "channels." In the very first block of our network, the input is a black and white image, which is a matrix (i.e., a 2D tensor). Our black and white images thus have one channel. Each filter output has dimension $h \times w \times 1$. If a building block uses multiple filters, their outputs are stacked together in the third dimension of the tensor so outputs have multiple channels, one channel corresponding to each filter. Therefore building blocks in the interior layers of our CNN take 3D tensors as inputs. If the input layer has multiple channels,

[7] This activation function, introduced by Maas et al. (2013), is defined as $\text{LeakyReLU}(x) = \begin{cases} x, \text{if } x \geq 0 \\ kx, \text{if } x < 0 \end{cases}$, where $k = 0.01$ is the coefficient that controls the angle of the negative slope. Leaky ReLU is an improved variant of the standard ReLU function that simply zeros out the unresponsive (negative) outputs while maintaining the stimulated ones. A drawback of ReLU is that when inputs are all positive, the gradients are either all positive or all negative, which introduces obstacles to the gradient descent in the training step. Another drawback of ReLU is that certain neurons may never activate because all gradients flowing through these units fall into the zero region of the ReLU function. Leaky ReLU resolves both issues.

Figure 6: Diagram of a Building Block

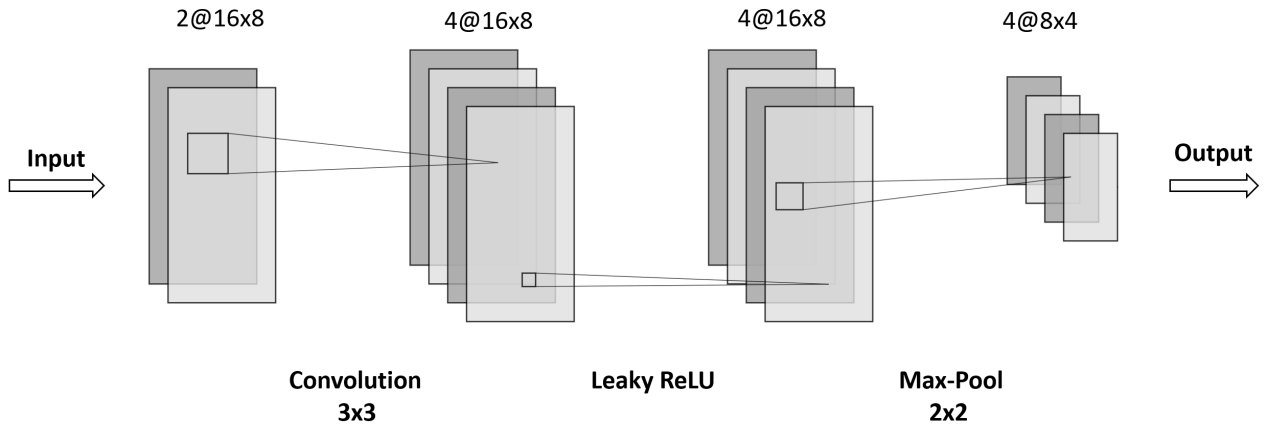

Note: A building block of the CNN model consists of a convolutional layer with 3×3 filter, a leaky ReLU layer, and a 2×2 max-pooling layer. In this toy example, the input has size 16×8 with 2 channels. To double the depth of the input, 4 filters are applied, which generates the output with 4 channels. The max-pooling layer shrinks the first two dimensions (height and width) of the input by half and keeps the same depth. Leaky ReLU keeps the same size of the previous input. In general, with input of size $h \times w \times d$, the output has size $h/2 \times w/2 \times 2d$. One exception is the first building block of each CNN model that takes the grey-scale image as input: the input has depth 1 and the number of CNN filters is 32, boosting the depth of the output to 32.

each filter of size (3×3) gains depth equal to the number of input channels, d (e.g., the filter is $3 \times 3 \times d$). Filters therefore aggregate input information locally in the height and width dimensions, but then combine this local information across all channels. In Figure 6, the input has height of 16 and width of 8 and has two channels. Thus each filter is $3 \times 3 \times 2$. The example uses four filters, so the size of the convolution output is $16 \times 8 \times 4$.

Within a building block, the output from all convolutional filters are fed element-wise through the leaky ReLU activation function, which preserves the dimensions of the convolution output. In the example, the ReLU activation output is therefore $16 \times 8 \times 4$. Finally, a max-pooling filter of size 2×2 with stride of two is applied to each channel separately, reducing their height and width by one-half each. The final output of the building block is $8 \times 4 \times 4$.

This output serves as the input to the next building block. By stacking many of these blocks together, the network first creates representations of small components of the image then gradually assembles them into representations of larger areas. The output from the last building block is flattened into a vector and each element is treated as a feature in a standard, fully connected feed-forward layer for the final prediction step. The final prediction is a linear combination of the vectorized image features, which is fed through a softmax (i.e., logistic) function to generate a probability of whether the future price will rise.

Figure 7: Diagram of CNN Models

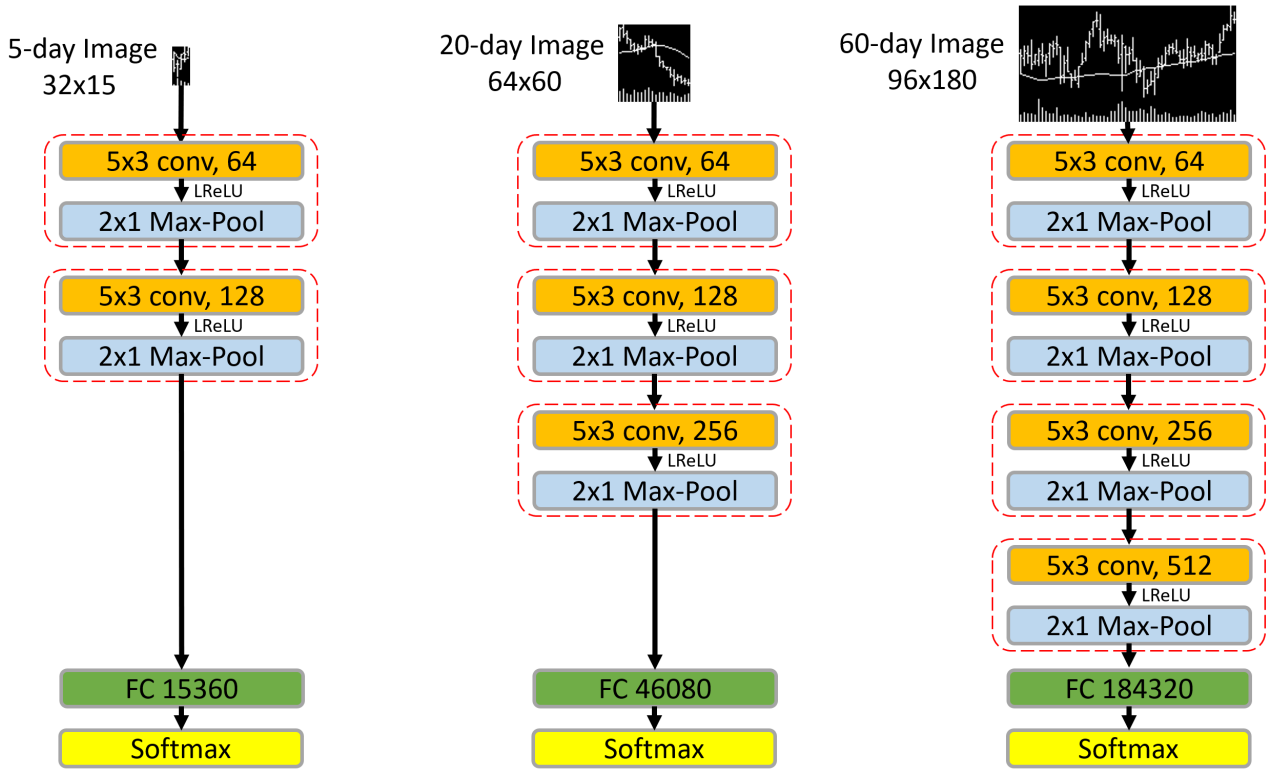

Note: This figure shows diagrams of 5-day CNN model (left), 20-day CNN model (middle), and 60-day CNN model (right). The 5/20/60-day CNN models are built with 2/3/4 CNN buidling blocks described in Figure 6. The notation D@HxW shows the output size of the CNN building block where H is the height, W is the width, and D is the depth (number of channels). The output of the last CNN block is flattened to a 1D vector and fed to a fully connected layer (FC), where the input size is calculated as the product $H \times W \times D$ from the last CNN building block. The final softmax layer yields the probabilities of up and down.

Having introduced the generic architectural components of CNN, we now discuss specific choices for our models. Since our images are largely sparse in the vertical dimension, we use 5×3 convolutional filters and 2×1 max-pooling filters. We use the same filter sizes in all layers for convenience. We use horizontal and vertical strides of 1 and 3 and vertical dilation rates of 2 and 3 for 20-day and 60-day images, respectively, only on the first layer because raw images are sparse. The number of CNN building blocks in our model is based on the size of the input image. We use 2 blocks to model 5-day images, 3 blocks for 20-day images, and 4 blocks for 60-day images. The number of filters for the first building block is 64 for all three models.[8] As pointed out by Zeiler and Fergus (2014), learned features become more complex in deeper layers, so we follow the literature and increase the number of filters after each convolutional

[8]We follow the popular VGG model (Simonyan and Zisserman, 2015) that uses 64 filters in its first layer.

Figure 8: Convolutional Filters that Detect the Next Day's Price Change

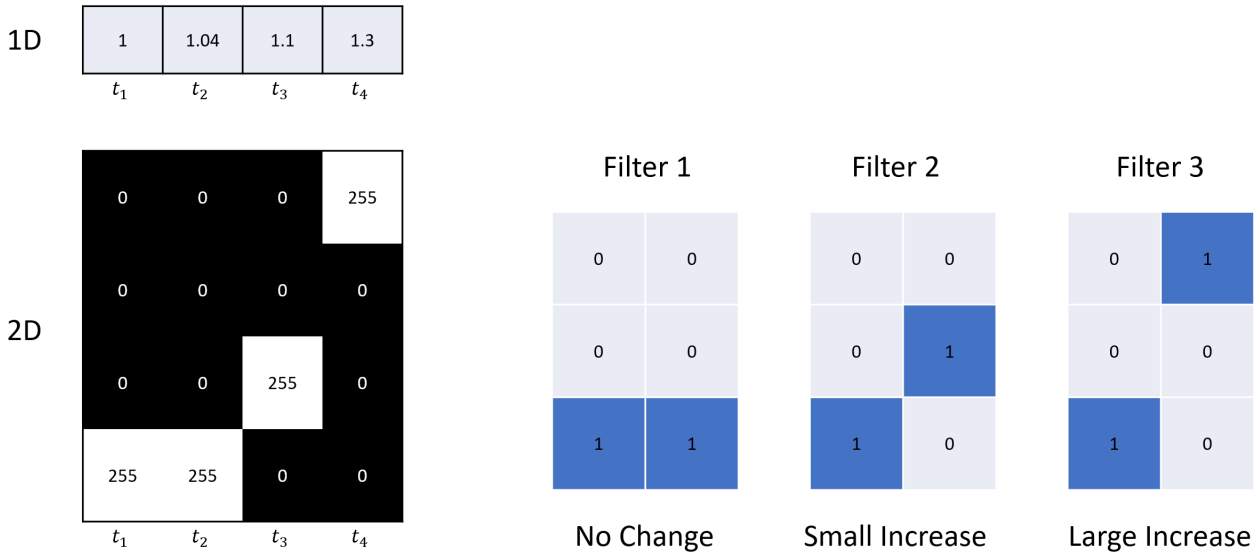

Note: A 1D data series represented as a 2D image, and filters for detecting no change, small increase, and large increase in price.

layer by a factor of two (e.g., 64, 128, 256, and 512 filters, respectively, in the four layers of the 60-day model). In turn, the fully connected layers have 15,360, 46,080, and 184,320 neurons for 5-day, 20-day, and 60-day models, respectively, which are determined by the outputs of the convolutional blocks. The total number of parameters are 155,138 for the 5-day model, 708,866 for 20-day, and 2,952,962 for 60-day models, respectively.[9] Of course, the effective parameterization of these models is much smaller than this parameter count due to heavy regularization that shrinks most parameters close to zero. The complete architecture for each model is shown in Figure 7.

3.2 Image Representation vs. Time-series Representation

Our research design recommends the counter-intuitive idea of embedding 1D time series data in a *higher* dimensional space, representing it as a 2D image, before bringing it to predictive analysis. Why is it beneficial to encode market data as an image, rather than directly modeling the 1D time series?

Raising the data representation to 2D makes it possible for a convolutional filter to capture

[9]The total number of parameters is calculated by summing up the number of parameters in convolutional layers and the number of parameters in the fully connected layer. The number of parameters in a convolutional layer is calculated as $(K^2 \times D + 1) \times F$, where K is the size of filters (fixed as 3 in our models), D is the depth (number of channels) of the input, and F is the number of filters. The number of parameters in a fully connected layer is calculated as $L \times 2$, where L is the length of the input vector and 2 corresponds to the two classification labels. We ignore the number of parameters from the batch normalization as it is negligible.

non-linear spatial associations among various price curves. Figure 8 is a simple example of how this works. It shows a price plot over four periods. In the first two periods the price is flat, in the third period it rises by one unit, and in the fourth period the price jumps by two units. A 1D kernel filter can only extract the linear difference between prices on two consecutive days without the further help of a non-linear activation function. If a price rise of two units is more than twice as predictive as a price rise of one unit, the 1D kernel is unable to account for it. But a 2D CNN applied to the price plot image can. The example shows how this is achieved with 3×2 filters that treat "no change," "small increase," and "large increase" as separate features that can enter into an ultimate prediction with distinct weights. That is, when these filters are applied to 2D images, they act as indicator functions that detect and bin price movements of different sizes.

Likewise, as discussed in our discussion of price plot format in Section 2, the image automatically combines information on both directional price movements, movements relative to moving average trend, price volatility, and trading volume in a single representation. To jointly consider price direction and volatility, for example, a traditional time series model would require restrictive choices to manually engineer features. And incorporating volatility information would inevitably require non-linear transformations of price series along the lines of stochastic volatility or GARCH models. Fortunately, 2D CNN eliminates any need to manually engineer such features and instead extracts predictive patterns from the market data series within the CNN itself.

In short, ingesting data in the form of an image allows the model to isolate data relationships that may be difficult to detect with time series methods. Just as humans find it easier to detect patterns graphically rather than with lists of numbers, a statistical pattern recognition algorithm may also benefit from visualizing an entire data matrix in a single image.

3.3 Training the CNN

Our workflow from training, to model tuning, and finally to prediction follows the basic procedure outlined by Gu et al. (2020). First, we divide the entire sample into training, validation, and testing samples. In our main US data sample, we estimate and validate the model using a single eight-year sample at the start of our sample. In this eight-year sample, we randomly select 70% images for training and 30% for validation. Randomly selecting the training and validation sample helps balance positive and negative labels in our classification problem, which attenuates a potential bias in classification due to extended periods of bullish or bearish market swings. The remaining nineteen years of data comprise the out-of-sample test data set.

We treat the prediction analysis as a classification problem. In particular, the label for

an image is defined as $y = 1$ if the subsequent return is positive and $y = 0$ otherwise. The training step minimizes the cross-entropy loss, which is the standard objective function for classification problems. It is defined as:

$$L(y, \hat{y}) = -y \log(\hat{y}) - (1 - y) \log(1 - \hat{y}), \tag{1}$$

where $\hat{y}$ is the softmax output from the final step in the CNN. If the predicted probability exactly corresponds with the label, $\hat{y} = y$, then the loss function is zero, otherwise the loss is positive.

We adopt the same regularization procedures in Gu et al. (2020) to combat overfit and aid efficient computation. We apply the Xavier initializer for weights in each layer (Glorot and Bengio, 2010). This promotes faster convergence by generating starting values for weights to ensure that prediction variance begins on a comparable scale to that of the labels. Loss function optimization uses stochastic gradient descent and the Adam algorithm (Kinga and Adam, 2015) with initial learning rate of 1×10^{-5} and batch size of 128. We use a batch normalization (Ioffe and Szegedy, 2015) layer between the convolution and non-linear activation within each building block to reduce covariate shift.[10] We apply 50% dropout (Srivastava et al., 2014) to the fully connected layer (the relatively low parameterization in convolutional blocks avoids the need for dropout there). Finally, we use early stopping to halt training once the validation sample loss function fails to improve for two consecutive epochs. Gu et al. (2020) outline the intuition behind these choices, so for the sake of brevity, we omit this discussion and instead refer interested readers there.

In Appendix C, we design simulation experiments to investigate the finite sample performance of the CNN classifier. Since our images look rather different from standard CNN research data sets like ImageNet, the simulation evidence provides insight into the effectiveness of a CNN in this new environment. The general conclusion from simulations is that the CNN successfully detects complicated technical patterns in realistically low signal-to-noise data sets.

4 CNN Prediction for US Stock Returns

4.1 Data

We use daily stock data from CRSP for all firms listed on NYSE, AMEX, and NASDAQ. Our sample runs from 1993–2019 based on the fact that daily opening, high, and low prices first

[10] We also normalize all images using the mean and standard deviation of all pixel values from images in the training data, which are then used to normalize the validation and testing images. We adopt it as a standard operation in the CNN literature, though skipping this step has negligible impact on our results.

become available in June 1992.

Our price trend analysis focuses on returns adjusted for corporate actions by using returns to construct a price series. In each image, we normalize the first day closing price to one, and construct each subsequent daily close from returns (RET_t) according to[11]

$$p_{t+1} = (1 + RET_{t+1})p_t.$$

Each day's opening/high/low price levels are scaled in proportion to that day's closing price level.

We consider three input choices that include images of market data over the past 5, 20, or 60 days. Image labels take a value of one or zero for positive or non-positive returns over the 20 or 60 days subsequent to the image. Thus, our main analysis amounts to six separately estimated models. In an extension we also study short-horizon prediction based on returns over the 5 days subsequent to the image. Because the CNN optimization is stochastic, for each model configuration we independently re-train the CNN five times and average their forecasts (following Gu et al., 2020).

Some important considerations when reading our empirical results are that *we do not recursively re-train the model* and that we *randomly* select training and validation samples. Specifically, we train and validate each model only once using data from 1993 to 2000, in which 70% of the sample are randomly selected for training and the remaining 30% for validation. The trained CNN model is then held fixed for the entire 2001 to 2019 test sample.

4.2 Classification Accuracy

The CNN targets a binary outcome equal to one for a positive return over the specified forward horizon and zero otherwise. The fitted value from the CNN is an estimate for the probability of a positive outcome. A true positive (TP) or true negative (TN) occurs when a predicted "up" probability of greater than 50% coincides with a positive realized return and a probability less than 50% coincides with a negative return. False positives and negatives (FP and FN) are the complementary outcomes. We calculate classification accuracy as

$$\text{Accuracy} = (TP + TN)/(TP + TN + FP + FN).$$

Table 2 summarizes the CNN's out-of-sample classification accuracy at the stock level. For all image sizes (5, 20, and 60 days) and forecast horizons (20 and 60 days), CNN accuracy significantly exceeds that of a random guess (0.5) with a p-value below 0.01 (with the exception

[11] An earlier version of this paper used the ex-dividend return $RETX_t$ to build the price series according to $p_{t+1} = (1 + RET_{t+1})p_t$. This gives nearly identical results to using RET_t.

Table 2: Out-of-Sample Classification Accuracy

	Return horizon			
	20-day		60-day	
Image size	Acc.	Corr.	Acc.	Corr.
5-day	52.5%	3.1%	53.6%	2.3%
20-day	53.3%	3.4%	53.2%	2.4%
60-day	53.6%	2.9%	52.9%	3.1%
MOM	52.1%	1.8%	52.1%	1.5%
STR	50.4%	1.4%	49.8%	1.2%
WSTR	51.0%	2.8%	50.4%	2.6%

Note: The table reports out-of-sample forecast performance for image-based CNN models and benchmark signals. We calculate classification accuracy and correlation cross-sectionally each period then report time series averages over each period in the test sample.

of accuracy for STR, all statistics in the table are significant, so we suppress p-values). For comparison we also report classification accuracy based on more traditional stock predictors. In particular, we look at momentum (MOM) measured as the average return over the two to twelve months prior to the forecast, short-term reversal (STR) measured as the one-month return prior to the forecast, and weekly short-term reversal (WSTR) measured as the one-week return prior to the forecast. For benchmark signals like MOM, we calculate accuracy by following the convention in the literature and defining a signal as an "up" prediction if it exceeds the cross-sectional median value of the signal. MOM and WSTR are also statistically significant improvements over random guessing, and both are less accurate than the best CNN at each horizon.

Note that seemingly minor improvements in accuracy can translate into large gains in portfolio performance. Appendix A provides a derivation demonstrating that for every 0.5% increase in accuracy, there is a corresponding gain in annualized Sharpe ratio of roughly 0.1 for an investor that exploits the classifier for a timing strategy. In a calibrated example, improving monthly prediction accuracy from 52% to 53% can raise the timing strategy's annualized Sharpe ratio from 0.6 to 0.8.

The table also reports the time series average of cross-sectional correlations between each signal and subsequent realized returns. CNN forecasts achieve higher correlations than the benchmark signals on average. The CNN's improvements over MOM and STR are statistically significant, but differences versus WSTR are insignificant.

4.3 Portfolio Performance

Portfolio analysis provides more detailed insight into CNN forecast accuracy. Average accuracy and return correlation provide a single aggregate summary of forecast performance. But

Figure 9: Prediction Accuracy By Decile

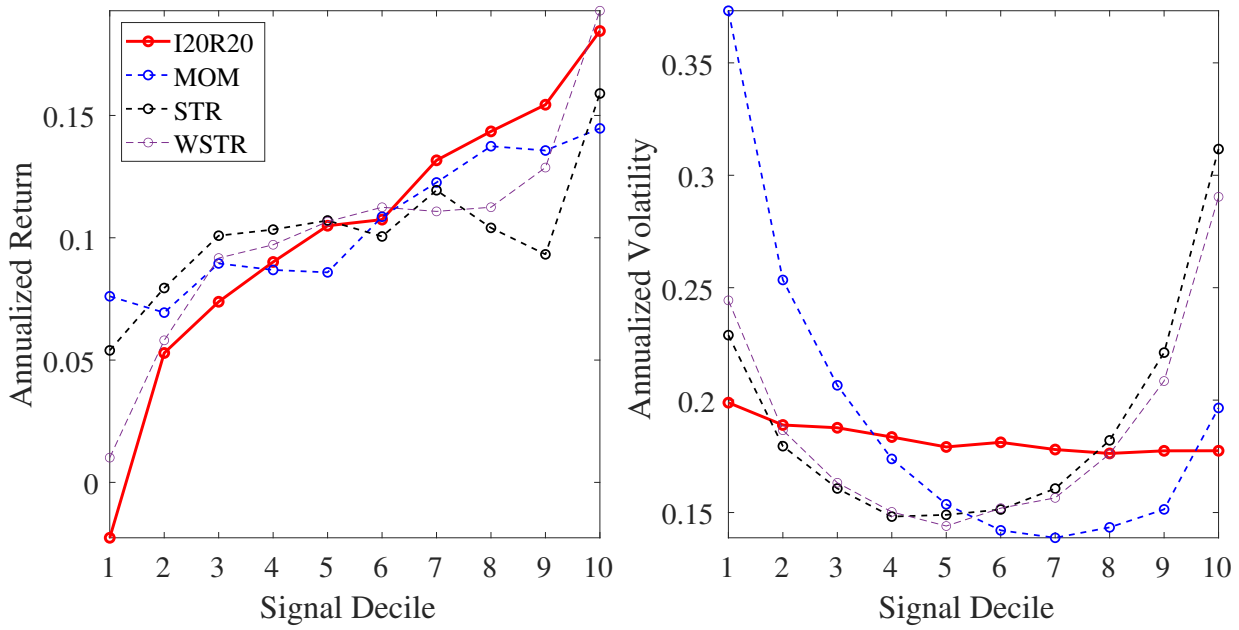

The left figure reports average realized returns in each decile of I20R20 CNN model forecasts and for each decile of the benchmark signals. Return averages are based on cross-sectional decile averages each period that are then averaged over time. The right figure shows the time series volatility of decile returns.

by studying realized returns at different quantiles of model predictions, we can understand accuracy across the full distribution of CNN forecasts. For example, the left panel in Figure 9 shows the average 20-day realized return at each decile of the CNN forecast distribution (based on 20-day images, denoted "I20R20" in the figure), first averaged within deciles each period, then averaged over time (i.e., average returns of equal weight decile portfolios). To illustrate the precision of forecasts, the right panel shows the time series standard deviation of average decile returns. More positive CNN forecasts translate more or less monotonically into higher returns on average. This is also true for MOM, STR, and WSTR, though with a somewhat flatter slope. An interesting difference between CNN forecasts and other benchmark price trend signals is in their variability. All CNN decile portfolios have annualized volatility below 20%. Volatilities of MOM, STR, and WSTR realizations reach 30% to 35% in extreme deciles.

As our next analysis shows, the comparatively high accuracy and low variability of CNN forecasts in the example of Figure 9 translates into uniformly large trading improvements for image-based CNN strategies relative to benchmarks. Every period in which we construct new forecasts (monthly or quarterly, depending on the model's forecast horizon), we sort stocks into equal weighted decile portfolios based on out-of-sample CNN estimates for probability of

Table 3: Performance of Equal Weight Portfolios

	I5/R20		I20/R20		I60/R20		MOM/R20		STR/R20		WSTR/R20	
	Ret	SR	Ret	SR	Ret	SR	Ret	SR	Ret	SR	Ret	SR
Low	-0.00	-0.03	-0.02	-0.12	-0.02	-0.07	0.07	0.20	0.05	0.23	0.01	0.03
2	0.05	0.28	0.05	0.28	0.06	0.28	0.07	0.27	0.08	0.44	0.06	0.31
3	0.07	0.41	0.07	0.39	0.09	0.44	0.09	0.43	0.10	0.63	0.09	0.56
4	0.07	0.40	0.09	0.49	0.10	0.52	0.09	0.50	0.10	0.70	0.10	0.65
5	0.10	0.53	0.11	0.59	0.11	0.60	0.09	0.56	0.11	0.72	0.11	0.74
6	0.11	0.59	0.11	0.59	0.13	0.73	0.11	0.76	0.10	0.66	0.11	0.74
7	0.11	0.60	0.13	0.74	0.13	0.73	0.12	0.88	0.12	0.74	0.11	0.71
8	0.14	0.73	0.14	0.81	0.13	0.79	0.14	0.96	0.10	0.57	0.11	0.64
9	0.16	0.85	0.15	0.87	0.14	0.85	0.14	0.90	0.09	0.42	0.13	0.62
High	0.21	1.09	0.18	1.04	0.14	0.99	0.14	0.74	0.16	0.51	0.19	0.66
H-L	0.22***	2.35	0.21***	2.16	0.16***	1.29	0.07	0.25	0.11**	0.55	0.18***	1.23
Turnover	175%		173%		155%		63%		168%		167%	
	I5/R60		I20/R60		I60/R60		MOM/R60		STR/R60		WSTR/R60	
	Ret	SR	Ret	SR	Ret	SR	Ret	SR	Ret	SR	Ret	SR
Low	0.07	0.31	0.08	0.32	0.08	0.27	0.11	0.25	0.07	0.27	0.06	0.22
2	0.10	0.43	0.10	0.41	0.09	0.37	0.10	0.33	0.11	0.50	0.11	0.46
3	0.10	0.48	0.11	0.48	0.11	0.46	0.12	0.50	0.12	0.65	0.11	0.55
4	0.11	0.49	0.12	0.53	0.12	0.52	0.12	0.57	0.11	0.66	0.11	0.63
5	0.11	0.53	0.12	0.54	0.12	0.55	0.11	0.63	0.12	0.73	0.12	0.73
6	0.13	0.58	0.12	0.57	0.12	0.57	0.12	0.70	0.12	0.65	0.12	0.69
7	0.13	0.60	0.12	0.60	0.14	0.68	0.12	0.71	0.13	0.68	0.12	0.67
8	0.13	0.62	0.12	0.61	0.14	0.72	0.13	0.81	0.12	0.54	0.12	0.58
9	0.13	0.62	0.13	0.70	0.14	0.75	0.13	0.78	0.12	0.45	0.13	0.52
High	0.16	0.77	0.13	0.74	0.15	0.88	0.13	0.57	0.14	0.40	0.16	0.48
H-L	0.09***	1.30	0.05	0.37	0.07*	0.43	0.02	0.06	0.07	0.34	0.10***	0.65
Turnover	59%		59%		58%		37%		56%		56%	

Note: Performance of equal-weighted decile portfolios sorted on out-of-sample predicted up probability. Each panel reports the average annualized holding period return and Sharpe ratio. Average returns accompanied by ***,**,* are significant at the 1%, 5% and 10% significance level, respectively. We also report monthly turnover of each strategy.

a positive subsequent return. We also construct a long-short spread portfolio ("H-L") that is long decile 10 and short decile 1. The holding period for each portfolio coincides with the forecast horizon for each model (either 20 or 60 days following the last date in an image). Throughout we use the notation "Ix/Ry" to denote that the model uses x-day images to predict subsequent y-day holding period returns.

Table 3 reports portfolio performance in terms of annualized average returns and Sharpe ratios. The top panel focuses on one month holding period strategies based on each image size (5, 20, or 60 days). Decile 1, which corresponds to stocks having the lowest probability of a positive future return indeed realize large negative Sharpe ratios of approximately -0.1 for all image sizes. Sharpe ratios increase monotonically across predicted "up" probability deciles. A long-only strategy based on stocks in decile 10 alone earns a Sharpe ratio of roughly 1.0

Table 4: Performance of Value Weight Portfolios

	I5/R20		I20/R20		I60/R20		MOM/R20		STR/R20		WSTR/R20	
	Ret	SR	Ret	SR	Ret	SR	Ret	SR	Ret	SR	Ret	SR
Low	0.05	0.31	0.05	0.28	0.06	0.32	0.01	0.03	0.04	0.21	0.02	0.07
2	0.05	0.29	0.04	0.21	0.05	0.24	0.02	0.08	0.06	0.38	0.05	0.26
3	0.05	0.30	0.05	0.32	0.07	0.42	0.04	0.18	0.06	0.36	0.05	0.30
4	0.07	0.44	0.05	0.33	0.10	0.55	0.07	0.35	0.08	0.57	0.06	0.44
5	0.06	0.42	0.06	0.40	0.05	0.32	0.07	0.43	0.09	0.61	0.09	0.62
6	0.08	0.48	0.08	0.50	0.07	0.41	0.08	0.56	0.09	0.60	0.09	0.60
7	0.07	0.46	0.08	0.51	0.08	0.48	0.09	0.64	0.11	0.68	0.11	0.78
8	0.09	0.56	0.09	0.58	0.09	0.59	0.10	0.73	0.10	0.57	0.10	0.63
9	0.09	0.56	0.08	0.55	0.07	0.48	0.10	0.69	0.08	0.37	0.10	0.51
High	0.10	0.65	0.11	0.67	0.09	0.62	0.14	0.67	0.05	0.18	0.07	0.27
H-L	0.05*	0.45	0.05**	0.49	0.02	0.17	0.12	0.36	0.01	0.03	0.06	0.30
Turnover	187%		181%		165%		76%		184%		185%	
	I5/R60		I20/R60		I60/R60		MOM/R60		STR/R60		WSTR/R60	
	Ret	SR	Ret	SR	Ret	SR	Ret	SR	Ret	SR	Ret	SR
Low	0.07	0.34	0.06	0.27	0.07	0.32	0.08	0.19	0.06	0.24	0.04	0.15
2	0.11	0.55	0.07	0.33	0.10	0.50	0.04	0.12	0.09	0.46	0.07	0.35
3	0.08	0.41	0.08	0.38	0.08	0.46	0.09	0.38	0.08	0.49	0.08	0.47
4	0.08	0.45	0.09	0.47	0.09	0.47	0.09	0.45	0.09	0.60	0.10	0.63
5	0.10	0.60	0.09	0.45	0.08	0.43	0.08	0.53	0.11	0.72	0.11	0.72
6	0.08	0.48	0.08	0.48	0.09	0.49	0.11	0.67	0.10	0.62	0.10	0.59
7	0.09	0.52	0.09	0.50	0.09	0.54	0.10	0.70	0.11	0.68	0.11	0.68
8	0.09	0.56	0.10	0.57	0.09	0.53	0.09	0.61	0.10	0.54	0.10	0.56
9	0.08	0.51	0.10	0.69	0.09	0.52	0.09	0.62	0.09	0.41	0.09	0.45
High	0.11	0.76	0.09	0.65	0.11	0.75	0.12	0.57	0.08	0.26	0.08	0.28
H-L	0.05**	0.47	0.04	0.32	0.03	0.23	0.04	0.10	0.02	0.08	0.04	0.19
Turnover	62%		60%		59%		42%		61%		62%	

Note: Performance of value-weighted decile portfolios sorted on out-of-sample predicted up probability. Each panel reports the average holding period return and annualized Sharpe ratios. Average returns accompanied by ***,**,* are significant at the 1%, 5% and 10% significance level, respectively. We also report monthly turnover of each strategy.

across CNN models. Long-short H–L strategies earn annualized Sharpe ratios of 2.4, 2.2, and 1.3 for CNN models based on 5-day, 20-day, and 60-day images, respectively. To benchmark these results, we also report performance of one month holding period strategies based MOM, STR, and WSTR, whose decile spreads earn annualized Sharpe ratios of 0.3, 0.6, and 1.2, respectively.

The table also reports the fraction of the strategy that turns over on average, scaled into *monthly* terms. Following Gu et al. (2020), we calculate monthly turnover as:

$$\text{Turnover} = \frac{1}{M}\frac{1}{T}\sum_{t=1}^{T}\left(\sum_{i}\left|w_{i,t+1} - \frac{w_{i,t}(1+r_{i,t+1})}{1+\sum_j w_{j,t}r_{j,t+1}}\right|\right),$$

where M is the number of months in the holding period, T is the number of trading periods, $r_{i,t+1}$ is the return of stock i at time $t+1$, and $w_{i,t}$ is the portfolio weight of stock i at time t. Dividing by the number of months makes the turnover measure comparable across the different holding periods that we investigate, for example scaling down quarterly strategy turnover by a factor of 1/3 or scaling up weekly strategy turnover by a factor of 5. A strategy that completely reconstitutes its holdings with no overlap from one holding period to the next will have maximum turnover of $200\%/M$ while a buy-and-hold strategy that never rebalances achieves minimum turnover of 0%.

MOM and STR H-L strategies with monthly holding periods are useful turnover benchmarks from the asset pricing literature with MOM typically viewed as a strategy that survives trading costs while STR does not. The monthly turnover of STR is 168% in our sample and MOM turnover is 63%. One-month holding period CNN strategies have essentially the same turnover as STR (and WSTR), but with more than three times the Sharpe ratio of STR and double the Sharpe ratio of WSTR. Momentum has substantially lower turnover than the monthly CNN strategy, but its Sharpe ratio is an order of magnitude smaller.

The bottom panel of Table 3 shows performance for quarterly holding period portfolios. Again the best performance is based on 5-day images, which produce a H–L Sharpe ratio of 1.3, followed by 0.4 for 20-day and 60-day images. Rebalancing once per quarter reduces CNN strategy turnover to roughly 60% per month, similar to that achieved from momentum with monthly rebalance. But, despite its comparable turnover, the CNN strategy's annualized Sharpe ratio of 1.3 is roughly five times larger than the one-month holding period momentum strategy. With a quarterly holding period, the Sharpe ratio of momentum drops to 0.1, while STR and WSTR earn 0.3, and 0.7, respectively.

In Table 4 we conduct the same analysis using value weights rather than equal weights. For one-month holding periods, CNN strategies deliver out-of-sample H-L Sharpe ratios of 0.5, 0.5, and 0.2, versus 0.4, 0.0, and 0.3 for MOM, STR, and WSTR, respectively. This demonstrates the well known robustness of MOM for value-weight strategies, and the well known *lack* of robustness of STR, which is wiped out by the use of value weights and is consistent with the fact that STR's performance is driven by micro-cap stocks. CNN is thus an important contrast with STR because it continues to excel amid value weighting, illustrating that image data is predictive across the size spectrum. Finally, at the quarterly investment horizon, the only strategy delivering significant H–L returns is the CNN using 5-day images, which achieves a Sharpe ratio of 0.5, followed by insignificant 0.3 and 0.2 Sharpe ratios using 20- and 60-day images. The next best quarterly strategy is WSTR with an insignificant Sharpe ratio of 0.2, while the Sharpe ratio of MOM drops to 0.1.

Table 5: Exposure to Technical Analysis Factors

	Equal Weight		Value Weight	
	20-day	60-day	20-day	60-day
Mean Ret	1.73%	1.33%	0.45%	0.17%
t-stat	9.4	5.6	2.1	0.7
Alpha	1.86%	1.31%	0.82%	0.27%
t-stat	10.7	5.6	3.9	1.1
Mkt-Rf	-0.32	-0.29	-0.21	-0.16
t-stat	-7.3	-5.0	-4.0	-2.6
Momentum	0.01	0.16	0.04	0.11
t-stat	0.3	3.0	0.9	1.9
STR	-0.07	0.05	-0.09	-0.01
t-stat	-1.3	0.7	-1.4	-0.1
WSTR	0.37	0.60	-0.92	-0.10
t-stat	1.2	1.4	-2.5	-0.2
R^2	26.8%	20.7%	21.6%	9.2%

Note: The table shows time-series regression statistics on excess market return, momentum, and short-term reversal (from Ken French's data library) and weekly short-term reversal factors (constructed as the $H - L$ WSTR spread from Table 3). The columns show equal-weighted portfolio (EW) and value-weighted portfolio (VW) for 20-day and 60-day images, respectively.

Table 5 estimates the extent to which image-based strategy returns are explained by exposure to the market or to well known price trend strategies. For conciseness, we collapse the CNN portfolios from six down to two by taking the equal weighted average of all models with the same supervision window. Of the four control factors, the market portfolio is most significantly associated with image-based strategies. After accounting for their negative betas, image-based alphas rise slightly above the raw average return. The primary conclusion from the table, however, is that image strategies bear little in common with well known momentum or reversal phenomena, and that these well known strategies are not responsible for the success of the CNN strategy.

4.4 Short-Horizon Predictions

In this subsection we analyze the predictive strength of the CNN at shorter horizons of one week. Short horizon prediction is interesting in our setting for understanding the predictive strength of image-based signals in intuitive economic terms (while recognizing that trading such an investment strategy would be costly). But it also lays the groundwork for us to explore the possibility that technical patterns in high frequency price data might manifest in similar forms at lower frequencies. After all, one of the most challenging aspects of empirical asset

Table 6: Short-horizon (One Week) Portfolio Performance

	Equal Weight											
	I5/R5		I20/R5		I60/R5		MOM/R5		STR/R5		WSTR/R5	
	Ret	SR	Ret	SR	Ret	SR	Ret	SR	Ret	SR	Ret	SR
Low	-0.28	-1.92	-0.32	-1.94	-0.21	-1.10	0.15	0.44	-0.01	-0.03	-0.08	-0.34
2	-0.04	-0.27	-0.04	-0.21	0.02	0.12	0.10	0.44	0.06	0.35	0.04	0.24
3	0.03	0.15	0.04	0.20	0.07	0.35	0.10	0.50	0.09	0.58	0.08	0.48
4	0.08	0.41	0.08	0.43	0.11	0.58	0.10	0.57	0.10	0.67	0.09	0.58
5	0.09	0.48	0.12	0.65	0.14	0.75	0.10	0.63	0.11	0.68	0.09	0.60
6	0.14	0.70	0.15	0.80	0.16	0.88	0.12	0.76	0.11	0.70	0.11	0.65
7	0.17	0.84	0.19	0.97	0.17	0.93	0.13	0.83	0.11	0.64	0.13	0.75
8	0.22	1.06	0.23	1.19	0.20	1.08	0.14	0.90	0.12	0.62	0.14	0.72
9	0.30	1.48	0.27	1.40	0.22	1.23	0.15	0.91	0.16	0.68	0.18	0.81
High	0.54	2.89	0.52	2.76	0.33	1.85	0.16	0.78	0.38	1.19	0.46	1.56
H-L	0.83***	7.15	0.84***	6.75	0.54***	4.89	0.02	0.07	0.39***	1.76	0.53***	2.84
Turnover	862%		834%		774%		154%		426%		825%	
	Value Weight											
	I5/R5		I20/R5		I60/R5		MOM/R5		STR/R5		WSTR/R5	
	Ret	SR	Ret	SR	Ret	SR	Ret	SR	Ret	SR	Ret	SR
Low	-0.03	-0.19	-0.03	-0.16	-0.02	-0.12	0.03	0.06	0.04	0.16	-0.02	-0.09
2	0.00	0.00	0.02	0.12	0.01	0.06	0.02	0.05	0.04	0.22	0.03	0.14
3	0.04	0.24	0.04	0.24	0.04	0.24	0.07	0.27	0.06	0.34	0.06	0.34
4	0.06	0.35	0.06	0.32	0.06	0.31	0.08	0.36	0.09	0.54	0.06	0.36
5	0.06	0.34	0.06	0.34	0.06	0.34	0.08	0.41	0.09	0.57	0.08	0.48
6	0.09	0.50	0.09	0.51	0.06	0.32	0.08	0.46	0.10	0.57	0.10	0.60
7	0.11	0.58	0.09	0.49	0.08	0.45	0.08	0.51	0.10	0.51	0.11	0.63
8	0.12	0.62	0.11	0.61	0.09	0.49	0.10	0.62	0.13	0.63	0.15	0.73
9	0.16	0.81	0.11	0.59	0.11	0.61	0.11	0.62	0.13	0.51	0.18	0.72
High	0.20	0.91	0.20	0.99	0.14	0.77	0.14	0.63	0.16	0.46	0.18	0.59
H-L	0.23***	1.49	0.22***	1.74	0.16***	1.44	0.12	0.33	0.13*	0.44	0.21***	0.77
Turnover	947%		910%		839%		204%		541%		917%	

Note: Performance of equal-weighted (top panel) and value-weighted (bottom panel) decile portfolios sorted on out-of-sample predicted up probability. Each panel reports the average holding period return and annualized Sharpe ratios. Average returns accompanied by ***,**,* are significant at the 1%, 5% and 10% significance level, respectively. We also report monthly turnover of each strategy.

pricing is the dearth of time series data. The finance literature focuses most often on monthly data because the most economically important patterns in asset markets unfold over monthly or lower frequencies. Yet we experience only one history of financial market prices, meaning that we have at most several hundred monthly time series observations and several dozen annual observations. Given the scarcity of low frequency data, it would be greatly beneficial to know if patterns that unfold at high frequencies (which we can potentially measure well thanks to the availability of large high frequency data sets) are similar to patterns that unfold at low frequencies. This is Mandelbrot's (2013) hypothesis of "self-similarity" (also "scaling" or "fractal" behavior) in financial markets—i.e., that asset prices exhibit statistically similar patterns when studied at different time scales. Before studying the self-similar time scale hypothesis in detail in Section 5, we first report the behavior of CNN predictions at higher

Table 7: Other Holding Periods

	Holding Period					
	Equal Weight			Value Weight		
Model	5 days	20 days	60 days	5 days	20 days	60 days
I5/R5	7.15	2.77	1.40	1.49	0.77	0.46
I5/R20	5.53	2.35	1.36	1.26	0.45	0.31
I5/R60	4.32	2.05	1.30	0.74	0.32	0.47
I20/R5	6.75	3.17	1.59	1.74	0.73	0.37
I20/R20	3.87	2.16	1.05	0.89	0.49	0.44
I20/R60	0.97	0.45	0.37	0.01	0.26	0.32
I60/R5	4.89	2.33	1.08	1.44	0.55	0.35
I60/R20	2.19	1.29	0.60	0.99	0.17	0.13
I60/R60	1.00	0.75	0.43	0.36	0.38	0.23
Combo	4.07	1.92	1.02	0.99	0.46	0.34

Note: The table reports out-of-sample Sharpe ratios for holding periods of 5, 20, or 60 days with equal weight and value weight portfolios. All strategies use H-L decile spread portfolios sorted by image-based return predictions from each model.

frequencies than those reported above.

Table 6 reports the predictive strength of the CNN model when it targets 5-day ahead returns. We summarize predictive strength in the economic terms of one-week holding period portfolios. The CNN is especially adept in forecasting at this frequency. For equal weight portfolios (top panel), the weekly image-based strategy earns annualized Sharpe ratios ranging from 4.9 to 7.2. For comparison, the closest benchmark is WSTR with a Sharpe ratio of 2.8. In value weight portfolios, the CNN strategy earns a 1.4 to 1.7 Sharpe ratio, double the 0.8 Sharpe ratio for the value weight WSTR strategy.

Until now, all of our portfolio analyses have studied holding periods equal to the forecast horizon in each model (e.g., rebalancing positions every five days for I5/R5 but every 60 days for I5/R60). But there is no guarantee that the best quarterly trading portfolio, for example, comes from a model that was trained with 60-day returns. Table 7, studies the possibility that CNN models trained with one supervising return horizon are helpful for predicting different return horizons out-of-sample. To this end, we investigate portfolio performance for a range of holding periods (5, 20, or 60 days) regardless of the horizon of the supervising return. Indeed, we see that there is no single image length, and no single supervision window, that is dominant in terms of portfolio performance across investment horizons. For example, it is often the case that quarterly trading strategies benefit when the prediction model is supervised with shorter horizon returns. Furthermore, we find that image-based forecasts from different models pick

Figure 10: Trading Delay and Sharpe Ratio Decay

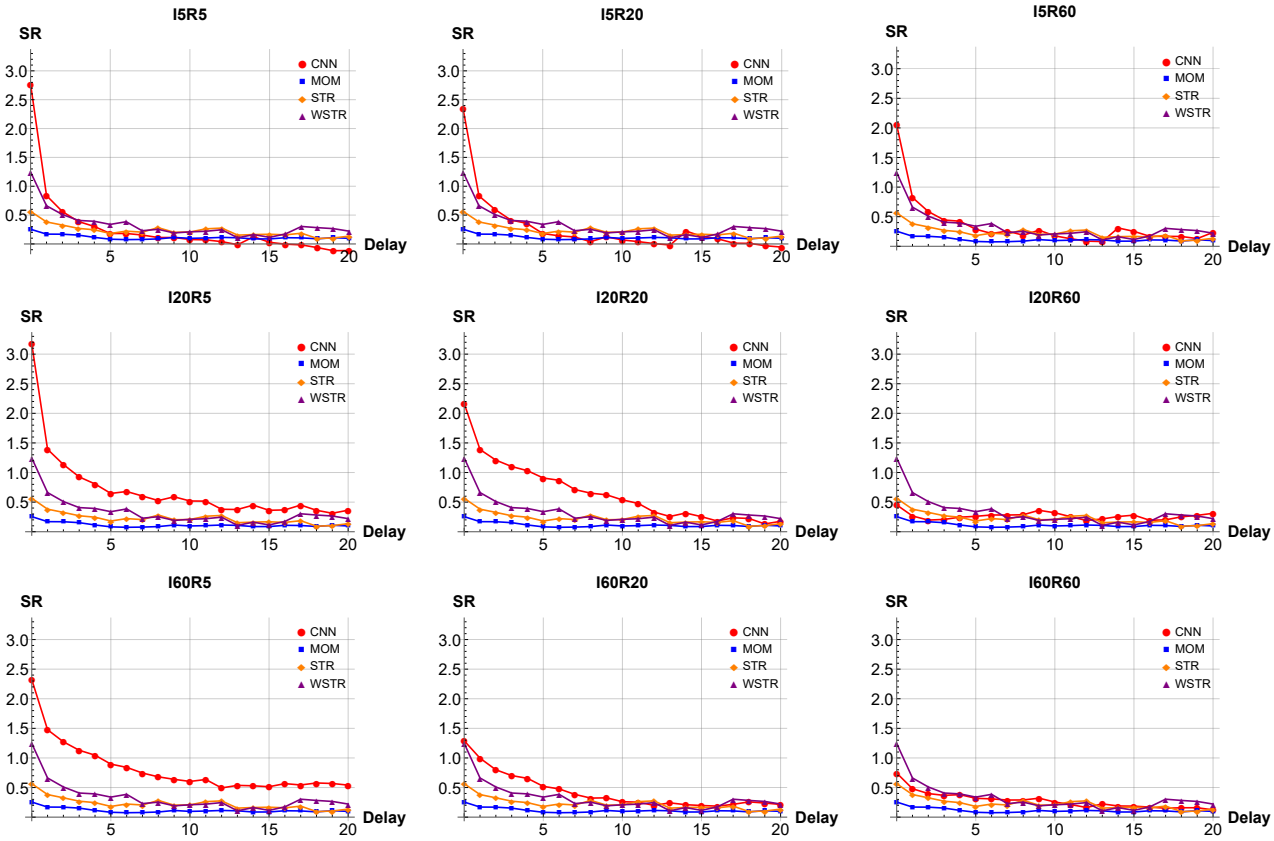

Note: The figures report out-of-sample annualized Sharpe ratios for equal-weight H-L decile spread strategies sorted on predictions from each CNN model, MOM, STR, and WSTR. All strategies use a 20-day holding period, but there is a delay in implementing the portfolio of $j = 0, 1, ..., 20$ days after the sorting characteristics becomes available (corresponding to the horizontal axis).

up on different signals. For example, the correlation between the I5R5 and I20R20 models is 32%. Pairwise correlations between all nine model configurations are below 50% on average and as low as 7% (and as high as 74%) between some models. This suggests that investment strategies can benefit from combining forecasts from multiple CNN models.

Table 6 indicates that trading strategy performance is strongest in the first week after portfolio formation. This, however, is not the only driver of monthly and quarterly trading performance shown in Tables 3, 4. Figure 10 shows the performance of strategies from each CNN using 20-day holding period portfolios, but delays the start of the investment by $j = 0, 1, ..., 20$ days after the end of the associated image. Indeed, very strong performance can be earned by the CNN in the first week of trading, especially when the model is trained based on 5-day images. But an interesting pattern emerges in the center column of Figure 10. For a given forecast horizon and holding period, the prediction horizon of CNN forecasts becomes

Figure 11: Comparison With Traditional Technical Indicators

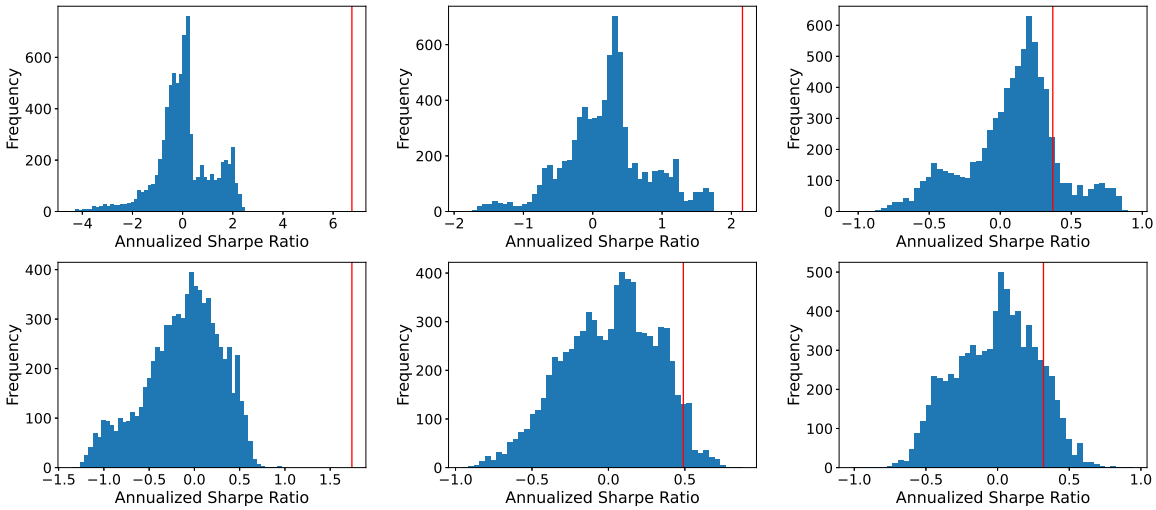

Note: The figure shows the histogram of Sharpe ratios for 7,846 technical analysis portfolios that rebalance by week, month, and quarter, respectively. The top panel shows equal weight portfolios and the bottom panel shows value weight portfolios. Red vertical bars are the corresponding Sharpe ratios for the I20/R5, I20/R20, and I20/R60 CNN strategies, respectively.

longer when large images are used. Moving from 5-day images to 20-day and then to 60-day images shows a flattening pattern in portfolio performance. Large images earn less in the first week, but more at longer horizons as they benefit from longer-range predictability. Strategies based on 20-day or 60-day images continue to earn Sharpe ratios around 1.0 or 0.5 even when the start of the investment is delayed by a week. And in these cases, the predictive strength of the CNN is longer-lived than the benchmark signals MOM, STR, and WSTR.

4.5 Traditional Technical Analysis

Brock et al. (1992) find that 26 pre-defined (and commonly used) technical trading rules generate significantly positive investment performance. Lo et al. (2000) introduce a kernel regression approach to recognizing technical indicators and find further support for the positive performance of investment strategies that rely on technical analysis.

Sullivan et al. (1999) assess a universe of 7,846 pre-defined technical trading rules while carefully controlling for multiple testing to control the likelihood of false positives. While they find that none of the Brock et al. (1992) strategies deliver significant positive performance in the post-publication sample, they find evidence of significant positive performance in their larger universe of trading rules. More recently, Bajgrowicz and Scaillet (2012) revisit the same universe of 7,846 rules and conclude that none are significant after controlling the false discovery rate.

The Sullivan et al. (1999) universe of 7,846 technical rules offers an excellent opportunity to calibrate the significance of our results. They constitute a null distribution for benchmarking other technical analysis strategies. To use these benchmarks, we apply each of the 7,846 trading rules stock-by-stock and produce a stock-level signal,[12] then construct decile spread long-short strategies in the same way that we build our long-short CNN strategy. We use technical signals at the end of each week, month, or quarter to rebalance, depending on the portfolio holding period, and consider equal weighting and value weighting. This gives us a distribution of performances for 7,846 different strategies against which we compare the CNN strategy.

Figure 11 reports the histogram of annualized Sharpe ratios for the 7,846 technical signals and the corresponding CNN strategy Sharpe ratio (red bars). At the weekly horizon, zero of the 7,846 outperform the CNN strategy (regardless of weighting scheme), and the closest technical indicator is outperformed by a large margin. At the monthly horizon, again none of the technical rules exceed CNN performance in equal weighted terms, and only 4.4% exceed CNN when value weighted. At the quarterly horizon, the outperformance of CNN diminishes somewhat, with 13.4% and 12.9% of technical rules outperforming CNN with equal and value weighting, respectively.

There are two considerations to bear in mind when interpreting the results of Figure 11. First, is that the CNN exceedance rates are not the same as p-values because the technical strategy distribution is not truly a null distribution. There may in fact be some true positives in the technical strategy universe, so in this sense the exceedance rate is more conservative than a p-value. Second, this point is especially relevant for long horizon (monthly and quarterly) return comparisons. The technical indicator literature has focused only on very short holding periods, typically of a single day. The fact that a non-trivial proportion of quarterly strategies produce annualized Sharpe ratios above 0.5 is a new and potentially interesting finding that warrants further investigation (though is beyond the scope of this paper).

4.6 Robustness

Appendix B reports a number of robustness analyses that support the main empirical findings presented above. In particular, we perform sensitivity analysis of the CNN prediction model to alternate choices in image representation (e.g., excluding volume data or moving average price line), model architecture (e.g., varying the number of filters in each layer or varying the number of layers), and estimation (e.g., different dropout or batch normalization schemes). Finally, we compare CNN models to alternative computer vision models including "HOG" and "HAAR" (whose model descriptions are also included in the appendix).

[12] We are grateful to Olivier Scaillet for sharing his code.

5 Transfer Learning

Our analysis to this point has focused on daily data for the US stock market. Training the CNN in this setting confers two advantages from data size. First, because the US stock market is the largest in the world, the CNN benefits from a wide cross section of observations. Second, our use of daily data extends the time series dimension of our data set by a factor of five compared to using weekly data and a factor of 20 compared to using monthly data. However, we may be interested in applying CNN forecasts in contexts for which re-training the CNN model is infeasible. For example, in order to isolate low frequency dynamics in returns, one may wish to use images of long past price histories and forecast several months into the future. This is likely to be prohibitive for a CNN due to the data requirements necessary to achieve a sufficiently well trained model. Likewise, we may be interested in forecasting returns in small or emerging markets where the cross section may contain only a few hundred stocks.

In this section, we explore the possibility of *transfer learning* for constructing accurate image-based forecasts in contexts with limited data. Transfer learning uses patterns identified in one context to guide analysis or prediction in a different context.[13] We show that the prediction patterns identified by the CNN from daily US stock data transfer well to other time scales and to international markets. In doing so, we show that it is possible to apply CNN models estimated in daily US data to construct profitable portfolios in other settings that preclude direct training of the CNN. At the same time, it provides an additional out-of-sample demonstration of reliable predictive power of image-based CNN forecasts.

5.1 Time Scale Transfer

Transfer learning provides a means of investigating the possibility that price patterns apply at multiple time scales. While it is difficult to effectively train a CNN using monthly or annual observations, we can apply our CNNs trained on daily data to data sampled at lower frequencies. We first consider transferring the I5/R5 CNN to the problem of using 20-day price histories to forecast future 20-day returns. To do so, we draw the 20-day price history using a 5-period OHLC chart by re-defining a "period" to be a 4-day interval. Each tick mark in an image now corresponds to four days of market data collapsed into a single observation, and a given OHLC bar show open, high, low, close over the 4-day interval. By down-sampling market data from once per day to once every four days, we can apply I5/R5 estimates to a 20-day image.

Panel A of Table 8 compares approaches to portfolio construction using 20-day price histories to make 20-day future return forecasts. The columns labeled "baseline" correspond

[13] See, e.g., Pan and Yang (2009) for a survey of the computer science literature on transfer learning.

Table 8: Time Scale Transfer I5/R5 to I20/R20

	Panel A: Equal Weight Portfolios							
	Baseline		Re-train		Transfer		Baseline+Transfer	
	Ret	SR	Ret	SR	Ret	SR	Ret	SR
Low	-0.02	-0.12	-0.02	-0.10	-0.01	-0.07	-0.04	-0.19
2	0.05	0.28	0.05	0.26	0.04	0.25	0.04	0.20
3	0.07	0.39	0.07	0.37	0.07	0.40	0.06	0.35
4	0.09	0.49	0.09	0.49	0.08	0.43	0.08	0.44
5	0.11	0.59	0.10	0.56	0.09	0.50	0.09	0.52
6	0.11	0.59	0.11	0.61	0.10	0.53	0.11	0.64
7	0.13	0.74	0.12	0.65	0.11	0.59	0.13	0.70
8	0.14	0.81	0.14	0.79	0.14	0.70	0.15	0.80
9	0.15	0.87	0.15	0.82	0.17	0.84	0.17	0.89
High	0.18	1.04	0.20	1.15	0.24	1.14	0.23	1.17
H-L	0.21***	2.16	0.22***	2.21	0.25***	2.14	0.26***	2.46
Turnover	173%		177%		176%		175%	
	Panel B: Value Weight Portfolios							
	Baseline		Re-train		Transfer		Baseline+Transfer	
	Ret	SR	Ret	SR	Ret	SR	Ret	SR
Low	0.05	0.28	0.06	0.38	0.03	0.22	0.04	0.24
2	0.04	0.21	0.06	0.36	0.05	0.34	0.05	0.32
3	0.05	0.32	0.05	0.34	0.06	0.42	0.04	0.27
4	0.05	0.33	0.08	0.53	0.05	0.35	0.05	0.30
5	0.06	0.40	0.07	0.42	0.07	0.46	0.06	0.40
6	0.08	0.50	0.08	0.50	0.08	0.50	0.07	0.45
7	0.08	0.51	0.08	0.54	0.09	0.56	0.07	0.45
8	0.09	0.58	0.09	0.58	0.11	0.66	0.10	0.61
9	0.08	0.55	0.10	0.64	0.12	0.65	0.10	0.61
High	0.11	0.67	0.10	0.66	0.12	0.69	0.12	0.73
H-L	0.05**	0.49	0.04	0.33	0.09***	0.73	0.08***	0.67
Turnover	181%		187%		186%		184%	

Note: The table shows the performance of strategies using time scale transfer learning. In particular, we directly apply the I5/R5 CNN model estimated from daily data to construct forecasts from images that include 20 days of data sampled once every four days. Transfer learning portfolio performance (with a 20-day holding period) is reported under "Transfer." For comparison, we report a "Baseline" strategy that uses the I20/R20 CNN model of Tables 3 and 4, and a CNN model that is trained from scratch using images of 20 days of data sampled once every four days (under "Re-train"). Finally, "Baseline+Transfer" shows the performance of an equal-weighted average of the baseline and transfer strategies.

to CNN-based forecasts using daily data; i.e., it exactly repeats the strategy of the I20/R20 model in Table 3. The columns labeled "Re-train, No Transfer" re-estimate a CNN from scratch using 20 days of data collapsed into 5-period images and supervised by future 20-day returns. This provides a benchmark for how predictability is affected by simply down-sampling the price history and re-training the CNN. The columns labeled "Transfer" use estimates from the I5/R5 CNN to construct 20-day return forecasts from the collapsed 20-day images, thus

applying transfer learning at a 1:4 time scale.

Directly transferring the I5/R5 model to collapsed 20-day images with no re-estimation produces a remarkable 2.1 Sharpe ratio in equal weight portfolios. In this example, the transfer-based strategy performs nearly as well as the CNN re-trained with lower frequency data (whose Sharpe ratio is 2.2). Interestingly, the transfer learning signal is only 42% correlated with the baseline signal, indicating that they pick up in part on different predictive patterns. In the columns labeled "50/50 Baseline+Transfer" we show that differences in the information content from baseline and transfer signals can be leveraged to form an even stronger trading strategy. In particular, an equal weight combination of the two individual strategies returns a Sharpe ratio of 2.5. Panel B shows that when forming value weight decile portfolios, the transfer learning signal is in fact *more* powerful than the re-trained CNN. At 0.7, the H-L transfer strategy more than doubles the Sharpe ratios from re-training (0.3) and is around 50% larger than the baseline Sharpe ratio from daily data (0.5).

Next, we analyze 60-day market data collapsed into 5-period images (i.e., sampling once every 12 days) and forecasting returns over the next 60 days. We repeat the analysis of comparing the baseline I60/R60 strategy to either re-training the CNN on collapsed images, or directly transferring the estimated I5/R5 model to the I60/R60 problem at the 1:12 time scale. The results are reported in Table 9 and show that the comparative success of transfer learning becomes even more stark at this lower frequency time scale. In Panel A, we find that transfer achieves an H-L Sharpe ratio of 0.9 (for equally weighted portfolios), compared with the baseline I60/R60 Sharpe ratio of 0.4 and a re-training Sharpe ratio of 0.4. Value weight portfolios, reported in Panel B, also demonstrate success of the transfer approach with a Sharpe ratio of 0.3, versus a Sharpe ratio of 0.0 for re-training. The 50/50 combination of value weight baseline and transfer strategies reaches a Sharpe of 0.31, again demonstrating that transfer strategies applied at lower frequencies produce different and additive signals compared to the daily model (the gain in Sharpe ratio from the 50/50 combination is marginally significant at the 10% level).

5.2 International Transfer

International markets have fewer stocks and shorter time series compared to the US. If estimates from US data are applicable in international contexts, it helps alleviate the limitations of conducting data-intensive analysis in small markets. More generally, if predictive patterns in stock prices are to some degree global phenomena, then forecasts in data sparse markets can draw estimation strength from information in data rich markets. We explore the viability of international transfer learning by using CNN models estimated from US data to construct return forecasts in foreign markets.

Table 9: Time Scale Transfer I5/R5 to I60/R60

Panel A: Equal Weight Portfolios

	Baseline		Re-train		Transfer		Baseline+Transfer	
	Ret	SR	Ret	SR	Ret	SR	Ret	SR
Low	0.08	0.27	0.08	0.30	0.06	0.31	0.06	0.22
2	0.09	0.37	0.08	0.34	0.08	0.41	0.09	0.35
3	0.11	0.46	0.10	0.43	0.10	0.50	0.11	0.46
4	0.12	0.52	0.12	0.53	0.11	0.54	0.11	0.51
5	0.12	0.55	0.12	0.55	0.11	0.54	0.12	0.55
6	0.12	0.57	0.12	0.57	0.13	0.61	0.12	0.61
7	0.14	0.68	0.13	0.64	0.12	0.55	0.14	0.67
8	0.14	0.72	0.13	0.64	0.14	0.60	0.14	0.69
9	0.14	0.75	0.13	0.72	0.14	0.59	0.15	0.78
High	0.15	0.88	0.14	0.88	0.17	0.69	0.16	0.93
H-L	0.07*	0.43	0.06	0.37	0.10***	0.90	0.10***	0.81
Turnover	58%		59%		59%		58%	

Panel B: Value Weight Portfolios

	Baseline		Re-train		Transfer		Baseline+Transfer	
	Ret	SR	Ret	SR	Ret	SR	Ret	SR
Low	0.07	0.32	0.11	0.50	0.06	0.38	0.08	0.37
2	0.10	0.50	0.08	0.41	0.07	0.34	0.08	0.40
3	0.08	0.46	0.07	0.39	0.08	0.47	0.08	0.41
4	0.09	0.47	0.06	0.35	0.09	0.58	0.08	0.46
5	0.08	0.43	0.09	0.50	0.10	0.61	0.09	0.49
6	0.09	0.49	0.08	0.48	0.09	0.55	0.08	0.45
7	0.09	0.54	0.10	0.55	0.09	0.53	0.09	0.49
8	0.09	0.53	0.10	0.58	0.10	0.56	0.10	0.57
9	0.09	0.52	0.09	0.55	0.11	0.65	0.09	0.58
High	0.11	0.75	0.11	0.77	0.10	0.51	0.11	0.81
H-L	0.03	0.23	0.00	0.01	0.04	0.27	0.03	0.31
Turnover	59%		61%		62%		59%	

Note: The table shows the performance of strategies using time scale transfer learning. In particular, we directly apply the I5/R5 CNN model estimated from daily data to construct forecasts from images that include 60 days of data sampled once every 12 days. Transfer learning portfolio performance (with a 60-day holding period) is reported under "Transfer." For comparison, we report a "Baseline" strategy that uses the I60/R60 CNN model of Tables 3 and 4, and a CNN model that is trained from scratch using images of 60 days of data sampled once every 12 days (under "Re-train"). Finally, "Baseline+Transfer" shows the performance of an equal-weighted average of the baseline and transfer strategies.

We use daily stock market data from Datastream for Hong Kong, United Kingdom, Canada, Japan, Australia, Austria, Belgium, Denmark, Finland, France, Germany, Greece, Ireland, Italy, Netherlands, New Zealand, Norway, Portugal, Singapore, Spain, Sweden, Switzerland, Russia, India, and South Korea; and we use daily stock market data from CSMAR for mainland China.[14] The date range for most countries matches the US sample, 1993

[14]For exposition, we refer to each of these markets as "countries," though Hong Kong is a special administrative region of China.

Table 10: International Transfer and H-L Decile Portfolio Sharpe Ratios (I20/R20)

		Equal Weight			Value Weight		
	Stock Count	Re-train	Direct Transfer	Transfer−Re-train	Re-train	Direct Transfer	Transfer−Re-train
Global	17206	-0.07	0.21	0.29	0.64	-0.25	-0.90
Japan	3056	0.61	0.99	0.37*	0.24	0.12	-0.12
Canada	2924	0.04	-0.07	-0.11	0.52	0.77	0.24
India	1861	0.99	0.66	-0.33	0.94	0.11	-0.83
UnitedKingdom	1783	0.19	-0.03	-0.21	0.66	0.32	-0.34
France	955	-0.36	0.81	1.17***	-0.42	0.30	0.72***
SouthKorea	911	0.89	0.59	-0.30	-0.26	0.75	1.01***
Australia	886	1.97	2.20	0.22	-0.22	0.61	0.83***
Germany	868	-0.26	0.08	0.34*	0.24	0.40	0.16
China	662	0.82	0.06	-0.77	0.39	0.07	-0.33
HongKong	543	1.63	1.48	-0.15	0.51	1.12	0.62***
Singapore	284	0.36	2.20	1.83***	0.24	0.98	0.74***
Sweden	260	0.30	1.43	1.13***	0.61	0.71	0.10
Italy	241	0.63	1.71	1.08***	-0.05	0.65	0.69***
Switzerland	240	-0.07	0.06	0.13	0.06	0.72	0.66***
Denmark	223	-0.17	0.92	1.08***	0.35	0.63	0.28
Netherlands	212	-0.40	-0.31	0.09	0.24	0.23	-0.01
Greece	201	-0.30	0.10	0.40**	0.07	0.36	0.29
Belgium	171	-0.19	0.81	1.00***	-0.21	0.48	0.69***
Spain	170	0.76	-0.24	-1.00	0.09	0.40	0.31*
Norway	169	-0.02	1.00	1.02***	-0.19	0.77	0.96***
Portugal	121	0.27	0.27	0.00	-0.02	0.51	0.53**
NewZealand	114	0.43	1.04	0.61***	0.56	0.51	-0.05
Finland	113	0.37	1.37	1.00***	-0.23	0.45	0.68***
Austria	110	-0.10	0.08	0.18	0.31	0.44	0.13
Ireland	75	-0.17	0.19	0.36*	0.46	0.65	0.19
Russia	53	-0.42	0.91	1.32***	-0.32	0.75	1.07***
Average	1274	0.29	0.69	0.40	0.19	0.50	0.31
Average (excluding Global)	661	0.30	0.70	0.40	0.18	0.53	0.36

Note: The table reports annualized out-of-sample Sharpe ratios for H-L decile spread portfolios within each country. We report the average monthly stock count by country, the image-based strategy from re-training the I20/R20 CNN using local data, and the image-based strategy directly transfers the I20/R20 model estimated in US data without re-training. Sharpe ratio gains (Transfer−Re-train) accompanied by ***,**,* are significant at the 1%, 5% and 10% significance level, respectively.

to 2019, with the exception of Russia, Greece, Finland, Ireland, and Sweden which start in 1999. While some markets such as Japan and Canada have samples of around 3,000 stocks each month on average, the median country has roughly 300 stocks.

Our transfer learning implementation directly applies estimated CNN models from the US sample to price images in foreign markets, with no re-training. We then conduct portfolio sorts country-by-country using transfer-based return forecasts and calculate out-of-sample Sharpe ratios for decile spread H-L portfolios. We assess the benefits of transfer learning by comparing with otherwise identical CNN models estimated using local image data for each foreign market. In the interest of brevity, we focus our analysis on I20/R20 and I5/R5 models.

Table 10 reports I20/R20 portfolio performance for each country in our international sample, ordered by the monthly average stock count in each country. The left side of the table shows results for H-L strategies based on equally weighted decile portfolios. We report per-

Table 11: International Transfer and H-L Decile Portfolio Sharpe Ratios (I5/R5)

		Equal Weight			Value Weight		
	Stock Count	Re-train	Direct Transfer	Transfer−Re-train	Re-train	Direct Transfer	Transfer−Re-train
Global	17206	0.18	5.20	5.03***	0.46	-3.05	-3.50
Japan	3056	3.56	5.68	2.12***	0.96	1.23	0.27
Canada	2924	9.01	12.12	3.11***	2.98	5.34	2.36***
India	1861	2.52	-1.46	-3.98	0.67	-1.08	-1.75
UnitedKingdom	1783	0.03	-0.23	-0.26	1.04	0.98	-0.06
France	955	2.47	4.09	1.63***	1.12	2.10	0.98***
SouthKorea	911	3.64	1.66	-1.97	1.74	2.39	0.65***
Australia	886	8.28	11.37	3.09***	2.78	3.48	0.70***
Germany	868	-0.29	2.43	2.72***	-0.01	2.93	2.94***
China	662	2.26	-2.19	-4.45	0.66	-0.95	-1.62
HongKong	543	1.97	5.35	3.37***	0.72	2.08	1.36***
Singapore	284	6.98	6.79	-0.20	2.48	3.94	1.46***
Sweden	260	5.43	6.99	1.56***	0.83	2.37	1.54***
Italy	241	2.14	3.55	1.40***	0.76	1.60	0.84***
Switzerland	240	0.48	0.67	0.19	1.30	2.62	1.33***
Denmark	223	1.94	3.56	1.62***	1.18	1.85	0.68***
Netherlands	212	-0.30	3.75	4.05***	0.11	1.67	1.56***
Greece	201	2.74	3.26	0.51**	0.98	1.88	0.90***
Belgium	171	0.73	4.34	3.60***	0.73	2.88	2.15***
Spain	170	1.62	0.28	-1.35	0.68	1.02	0.34*
Norway	169	0.79	3.38	2.59***	1.11	2.88	1.77***
Portugal	121	0.30	2.64	2.33***	0.93	1.40	0.47**
NewZealand	114	0.50	2.34	1.84***	0.65	1.19	0.54***
Finland	113	2.66	5.38	2.72***	0.95	2.55	1.60***
Austria	110	0.14	0.67	0.53**	0.66	1.05	0.39**
Ireland	75	0.47	1.80	1.34***	0.31	1.99	1.69***
Russia	53	-0.72	2.19	2.91***	-0.13	0.44	0.57***
Average	1274	2.21	3.54	1.34	0.99	1.73	0.75
Average (excluding Global)	661	2.28	3.48	1.19	1.01	1.92	0.91

Note: The table reports annualized out-of-sample Sharpe ratios for H-L decile spread portfolios within each country. We report the average monthly stock count by country, the image-based strategy from re-training the I5/R5 CNN using local data, and the image-based strategy directly transfers the I5/R5 model estimated in US data without re-training. Sharpe ratio gains (Transfer−Re-train) accompanied by ***,**,* are significant at the 1%, 5% and 10% significance level, respectively.

formance for the CNN forecasts trained from scratch on country-specific data, for forecasts based on direct application of the CNN model estimated in US data, and for the difference. The last row shows the simple average of each column.

In 19 out of 26 countries, transfer learning produces a Sharpe ratio gain over the locally re-trained model (for equal weight portfolios), and the gain is statistically significant in 14 of these. In 15 out of 26 countries, transfer from the US model produces a Sharpe ratio in excess of 0.5. This is only achieved in 8 countries for locally re-trained models. On average, transfer from the US model produces a Sharpe ratio of 0.7, more than doubling the performance of locally re-trained models.

The comparative gains from transfer versus local training are similar in value weight strategies, shown in the right three columns of the table. In this case the gain in Sharpe ratio from transfer learning is significantly positive for 13 out of 26 countries. On average, transfer from

Figure 12: Sharpe Ratio Gains From International Transfer

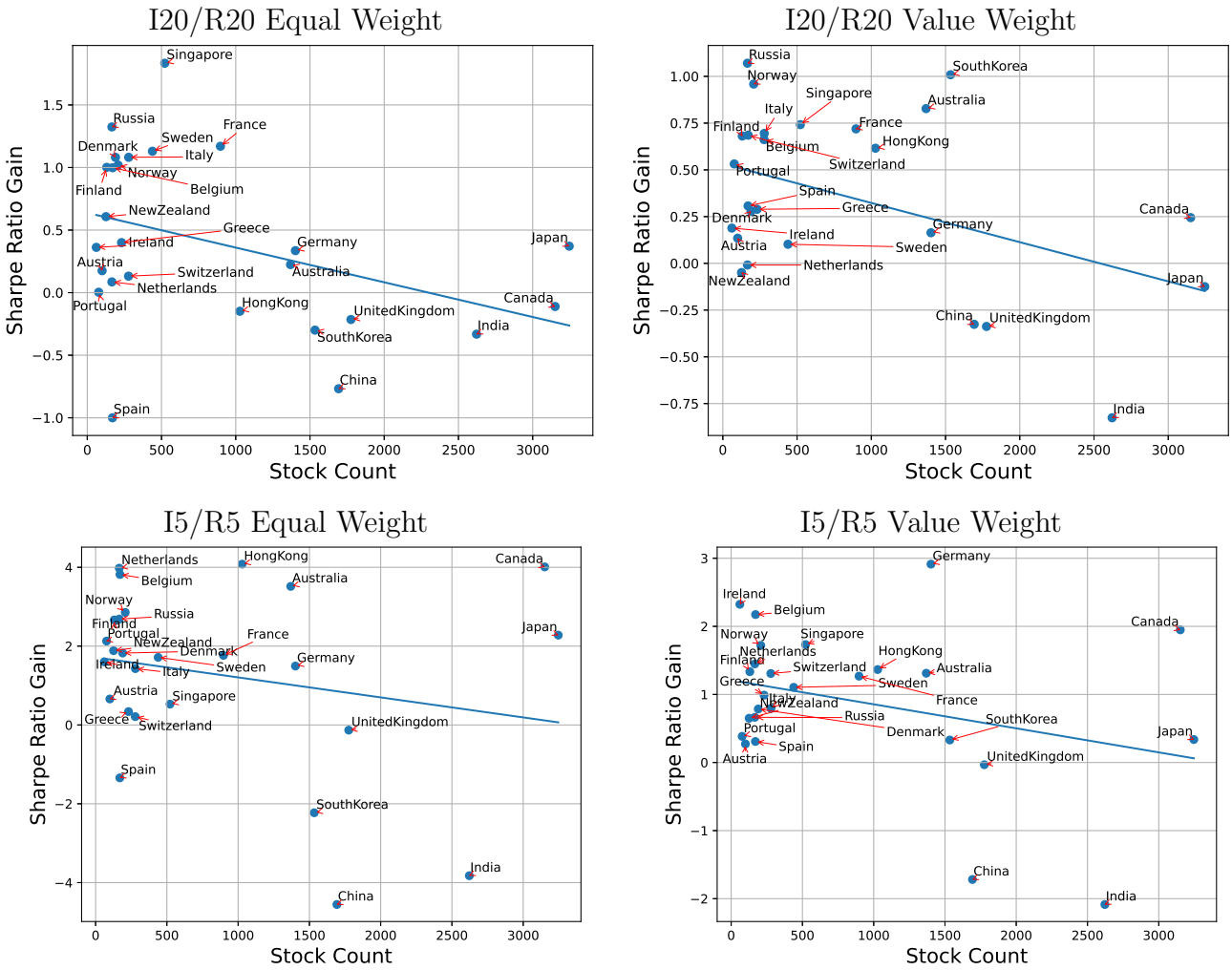

Note: The figures show annualized out-of-sample Sharpe ratio gains from I5/R5 and I20/R20 transfer learning (both equal-weight and value-weight strategies) versus the average number of stocks in each country.

US models more than doubles the Sharpe ratio of value weight strategies relative to locally re-trained models. The evidence is broadly similar and stronger for higher frequency forecasts, as shown in Table 11 for I5/R5 CNN models.

Figure 12 summarizes the benefits of international transfer learning by plotting the Sharpe ratio gains reported in Tables 10 and 11 against the number of stocks in each country. Most international markets are small and thus clustered on the left side of the plots. In these countries, portfolio Sharpe ratios tend to especially benefit from US transfer relative to locally trained CNN models. But for larger markets on the right side of the plots, the expected gains (based on the best fit line) are small or slightly negative. This suggests there are benefits to

Table 12: Correlation Between CNN Predictions and Stock Characteristics

CNN Model	MOM	STR	WSTR	Beta	Volatility	52WH	Bid-Ask	Dollar Volume	Zero Trade	Price Delay	Size	Illiq.
I5/R5	-0.00	-0.17	-0.34	0.05	-0.05	0.08	-0.03	0.13	-0.10	-0.03	0.12	-0.12
I5/R20	-0.01	-0.14	-0.32	0.05	-0.04	-0.04	-0.03	0.11	-0.09	-0.03	0.10	-0.11
I5/R60	0.04	-0.04	-0.11	0.01	-0.11	0.11	-0.10	0.15	-0.09	-0.03	0.16	-0.15
I20/R5	0.06	-0.09	-0.34	0.00	-0.13	0.13	-0.13	0.16	-0.07	-0.03	0.18	-0.17
I20/R20	0.10	0.04	-0.24	-0.01	-0.17	-0.15	-0.15	0.16	-0.05	-0.03	0.20	-0.18
I20/R60	0.13	0.21	-0.02	-0.01	-0.22	0.21	-0.20	0.25	-0.11	-0.05	0.29	-0.27
I60/R5	0.21	-0.06	-0.26	-0.05	-0.24	0.20	-0.25	0.20	-0.02	-0.03	0.27	-0.23
I60/R20	0.22	0.08	-0.11	-0.07	-0.26	-0.20	-0.25	0.20	-0.05	-0.03	0.28	-0.25
I60/R60	0.25	0.10	-0.01	-0.06	-0.28	0.23	-0.27	0.22	-0.01	-0.05	0.31	-0.26

Note: The table reports average cross-sectional correlations among model forecasts averaged over all period in the test sample.

local re-training when there is sufficient data, likely due to some degree of heterogeneity in predictive patterns across countries that transfer learning does not account for. A direction for further optimization of image-based prediction models would combine a global image model to capture shared differences with a country-specific model that accommodates some degree of heterogeneity. The model weights in this combination could be dictated by the relative informativeness of global and country-specific data in a Bayesian fashion.

6 What Does the CNN Learn?

Interpreting a CNN is difficult due to its recursive non-linear structure. We attempt to interpret the predictive patterns identified by the CNN using three approaches. First, we relate CNN fits to a collection of conceptually related (price, risk, and liquidity) signals widely studied in the literature. Second, we investigate regression-based linear approximations to the CNN using the data underlying the CNN's image input. Third, we use a CNN visualization method from the machine learning literature to understand how different image examples activate the regions of the CNN to trigger "up" or "down" return predictions. Our attempts at interpretation are admittedly incomplete (as in the CNN literature more broadly). Yet they achieve partial success by offering some visibility into the complex inner workings of the CNN model.

6.1 Association with Other Predictors

How unique are image-based forecasts compared to standard characteristics in the literature? We focus our comparison on measures of recent price trends (MOM, STR, WSTR, and

Table 13: CNN Predictions and Standard Stock Characteristics

	I5/R20	I20/R20	I60/R20
MOM	-0.05***	0.07***	0.41***
STR	-0.04***	0.42***	0.47***
Lag Weekly Return	-0.77***	-0.80***	-0.48***
Beta	0.12***	0.08***	0.10***
Volatility	-0.08***	-0.22***	-0.29***
52WH	0.04***	0.05***	0.05***
Bid-Ask	0.05***	0.05***	0.20***
Dollar Volume	0.05	-0.15***	-1.86***
Zero Trade	-0.02	0.18***	0.42***
Price Delay	-0.01	-0.02**	-0.01
Size	0.11***	0.59***	0.96***
Illiquidity	-0.25***	-0.35***	-2.10***
McFadden R^2	4.61	7.03	11.92

Note: The table reports slope coefficients and R^2 from panel logistic regressions of CNN model forecasts on stock characteristics. Panel regressions are estimated during the test sample using CNN models estimated in the training sample. Coefficients accompanied by ***,**,* are significant at the 1%, 5% and 10% significance level, respectively.

distance from 52-week high), risk (beta and volatility), and liquidity (bid-ask spread, dollar volume, number of no-trade days, price delay, size, and Amihud illiquidity).[15] Table 12 reports univariate correlations between each of these characteristics and each image-based forecast. We estimate period-by-period cross-sectional correlations among cross-sectional ranks of each variable, then report the time series average of correlation estimates during the test sample. Among the largest associations is WSTR, which has a correlation -26% to -34% for models supervised by future 5-day returns, consistent with the CNN picking up in part on a weekly short-term reversal pattern. The WSTR correlation drops close to zero when CNN models are supervised by 60-day returns. In a similar vein, MOM has its highest correlation (25%) with long-horizon forecasts from large images (I60/R60), but essentially zero correlation with short-horizon forecasts from small images (I5/R5). Image-based predictions from the CNN also resemble non-price firm characteristics. Other strong correlates are size, volatility, bid-ask spread, illiquidity, and dollar volume, all of which reach correlations near 30% and associate most strongly with forecasts from 60-day images.

These correlations are an impressive feat for the CNN. It shows that the CNN model has the ability to discern meaningful predictive information from data that is represented abstractly in the form of an image. MOM, STR, and other common price trend variations are predictive features that have been manually curated by human researchers over a decades long

[15]For variable definitions and references, see Table A.6 of Gu et al. (2020).

research process. But the CNN is oblivious to human-engineered features; instead, feature engineering is fully automated and integrated into the CNN model itself. Without requiring hand-crafted trend signals, the CNN still manages to identify trend-like features and liquidity features in the raw images.

Table 14: CNN, Future Returns, and Standard Stock Characteristics

	I5/R20			I20/R20			I60/R20		
CNN	0.37***		0.37***	0.54***		0.54***	0.46***		0.45***
MOM		0.17***	0.18***		0.17***	0.16***		0.17***	0.12***
STR		-0.02*	-0.01		-0.02*	-0.05***		-0.02	-0.09***
Lag Weekly Return		-0.19***	-0.07***		-0.19***	-0.05***		-0.19***	-0.13***
Beta		-0.05***	-0.05***		-0.05***	-0.05***		-0.05***	-0.05***
Volatility		-0.09***	-0.09***		-0.09***	-0.06***		-0.09***	-0.05**
52WH		-0.00	-0.01		-0.00	-0.02		-0.01	-0.03**
Bid-Ask		-0.13***	-0.13***		-0.12***	-0.14***		-0.12***	-0.17***
Dollar Volume		-0.08*	-0.09**		-0.08*	-0.09**		-0.08*	0.07*
Zero Trade		-0.02	-0.02		-0.02	-0.05**		-0.02	-0.07***
Price Delay		-0.00	-0.00		-0.00	-0.00		-0.00	-0.01
Size		0.16***	0.17***		0.17***	0.13***		0.17***	0.06
Illiquidity		-0.01	0.01		-0.01	0.02		-0.01	0.14***
McFadden R^2	0.84	0.12	0.93	1.73	0.12	1.79	1.23	0.12	1.30

Note: The table reports slope coefficients and R^2 from panel logistic regressions of future returns on image-based CNN model forecasts and standard stock characteristics. Panel regressions are estimated during the test sample using CNN models estimated in the training sample. Coefficients accompanied by ***,**,* are significant at the 1%, 5% and 10% significance level, respectively.

Table 13 shows the joint explanatory power for image-based predictions from all characteristics simultaneously (this table focuses on 20-day CNN predictions for brevity). We estimate a panel logistic regression using cross-sectional ranks of all regressors. In multiple regression, the significant predictors are MOM, STR, WSTR, volatility, 52WH, bid-ask spread, and size. The McFadden logistic R^2 ranges from 4.6% to 11.9%. So, while the CNN is able to detect signals within images that are significantly correlated with other well known predictors, the variation in image-based predictions is by and large unique.

Next, Table 14 reports logistic regressions of future stock returns on image-based forecasts while simultaneously controlling for the other characteristics. To remain comparable with the CNN model, the dependent variable is an indicator for a positive 20-day realized return. We estimate the regressions using only the test sample data (so that CNN parameters are estimated from an entirely distinct sample). For each CNN specification, we estimate three regressions, one using only the CNN forecast, one using stock characteristics and excluding the CNN forecast, and one joint regression using all predictors. We see that, across CNN models, the image-based prediction tends to be the strongest return forecaster. The McFadden R^2 due to image-based predictions alone ranges from 0.8% to 1.2% depending on the model configuration. The R^2 from all non-image based characteristics together is 0.1%. Coefficients on CNN image-based predictions are nearly identical in univariate and multivariate regressions.

Likewise, a large fraction of the predictive R^2 in the multivariate model is accounted for by the univariate CNN prediction, indicating that unique aspects of the CNN signal and not the previously studied characteristics drive the CNN's predictive power.

6.2 Image-Based Linear Approximation

What do the CNN models detect in images to produce accurate forecasts that are differentiated from traditional stock-level predictors? In this section, we use linear approximations of the CNN based on the raw market data that underlie our images. To do so, we must first decide on a representation of the price history data that is amenable for regression. The beauty of the CNN model, and the reason for its widespread usage in machine learning applications, is that it has the ability to extract predictive features from text with minimal data engineering on the part of the researcher. This contrasts with the standard approach from the momentum and reversal literature, which makes a number of human feature engineering choices—for example, representing historical data as returns rather than price levels to make series more comparable across assets. Our linear approximation analysis highlights the typical reliance on human feature engineering, because now we must also decide how to transform not only close prices, but also intra-day high and low prices, open prices, price moving averages, and volumes to make them relatable in the cross section.

To make linear regressions comparable with the image CNN model, we scale all price series such that the maximum of all prices appearing in the image (usually the maximum high price, but sometimes the maximum moving average price) is normalized to one and the minimum is normalized to zero. Daily volumes are likewise scaled by the maximum volume appearing in the image.

Our regressions focus on 5-day images. 5-day images contain relatively few data points (five observations each for open, high, low, and close price, volume, and moving average price), which makes them a convenient context for attempting to isolate image attributes that contribute to CNN success. In particular, there are few enough observations in a 5-day image that we can add each as a separate regressor in a linear model without risk of severe overfit.

Columns (1) through (3) of Table 15 pursue a linear approximation to the CNN forecast itself, as in Table 13. The dependent variable is the out-of-sample forecast generated by the CNN model for 5-day images, and the independent variables are data underlying 5-day images re-scaled to mimic the image representation. Across all return horizons (5, 20, and 60 days), the most important explanatory variables for the CNN forecast are the first lags of closing, high, and low prices, with the next most important variables being the first lag of trading volume and moving average price. These variables generally have consistent sign and magnitude for all return horizons. Compared to the first lag, lags two through five have a

Table 15: Linear Regressions Using Market Data With Image Scaling

	CNN as Dep. Var.			Positive Return Indicator as Dep. Var.								
	5D5P	5D20P	5D60P	5D5P			5D20P			5D60P		
	(1)	(2)	(3)	(4)	(5)	(6)	(7)	(8)	(9)	(10)	(11)	(12)
CNN				4.07*		4.28*	5.09*		6.27	6.07*		7.63*
open lag 1	-0.57*	0.01	0.29*		-0.23	-0.03		-0.07	-0.02		0.01	-0.07
open lag 2	0.27*	0.55*	0.22*		0.08	0.04*		0.12	0.02		0.05	-0.00
open lag 3	0.16*	-0.29*	-0.09*		0.05	0.01		-0.02	0.01		-0.13	-0.04
open lag 4	0.04*	-0.13*	-0.06*		0.02	0.00		-0.03	-0.00		-0.04	-0.01
open lag 5	0.10*	0.21*	0.45*		0.03	0.01		0.02	0.04		-0.04	-0.03
high lag 1	2.64*	0.99*	1.07*		0.61	0.11*		0.36	0.12		0.39*	-0.06
high lag 2	-0.27*	0.47*	0.77*		-0.07	-0.06		0.07	-0.05		0.13*	-0.18
high lag 3	-0.43*	-0.18*	-0.20*		-0.06	0.03*		-0.01	-0.00		0.07	0.05
high lag 4	-0.47*	-0.14*	-0.22*		-0.04	0.05*		0.04	0.02		0.03	0.05
high lag 5	-0.13*	0.31*	-0.38*		-0.05	0.01		0.09	0.02		0.03	-0.05
low lag 1	1.89*	0.94*	-0.06*		0.64	0.07*		0.23	-0.04		0.08*	0.14*
low lag 2	-0.17*	0.87*	0.74*		-0.08	-0.01		0.04	-0.09		0.15*	-0.06
low lag 3	-0.19*	-0.06*	-0.18*		-0.13	-0.04		-0.07	-0.00		0.02	0.09*
low lag 4	0.28*	0.41*	-0.13*		-0.03	-0.02		-0.02	-0.03		-0.02	0.03
low lag 5	-0.12*	-0.14*	-0.37*		-0.06	0.03*		-0.02	0.04		-0.08	0.11*
close lag 1	-5.36*	-3.91*	-2.19*		-1.23	0.01		-0.75	0.15		-0.58	0.23
close lag 2	0.72*	0.32*	0.19*		0.18	-0.02		0.13	0.04		0.01	-0.02
close lag 3	0.64*	0.83*	0.29*		0.10	0.01		0.14	0.05		-0.11	-0.07
close lag 4	0.73*	0.29*	0.20*		0.07	-0.00		0.12	0.10		0.02	-0.01
close lag 5	0.49*	0.55*	0.39*		0.09	0.01		0.11	0.07		-0.04	-0.01
ma lag 1	-1.33*	-1.06*	-0.56*		-0.16	0.00		-0.05	0.08		-0.14	0.02
ma lag 2	0.31*	0.35*	-0.01		-0.11	-0.16		-0.31	-0.50		0.13	-0.19
ma lag 3	-0.03*	-0.77*	0.20*		0.04	-0.03		0.08	0.06		0.43*	0.14
ma lag 4	-0.02	0.34*	0.63*		0.21	0.13*		-0.29	-0.10		-0.18	-0.06
ma lag 5	0.24*	-0.45*	-0.61*		-0.14	-0.06		0.09	0.10		-0.03	0.01
vol lag 1	0.81*	0.71*	0.42*		0.10	-0.03		0.08	-0.07		0.03	-0.11
vol lag 2	0.21*	0.52*	0.58*		0.00	-0.02		0.05	-0.05		0.05*	-0.10
vol lag 3	0.13*	0.15*	0.57*		0.00	-0.00		-0.01	-0.01		0.06*	-0.09
vol lag 4	-0.07*	0.12*	0.09*		-0.02	0.01		-0.02	-0.01		-0.05	-0.03
vol lag 5	0.05*	0.01	0.30*		-0.02	-0.01		-0.04	-0.01		-0.00	-0.01
McFadden R^2	35.29	33.32	21.96	1.35	0.99	1.38	0.94	0.58	0.99	1.56	0.50	1.69

Note: Results of logistic regressions on out-of-sample CNN forecasts and realized future return indicators on daily price and volume data. Panel regressions are estimated during the test sample using CNN models estimated in the training sample. Coefficients accompanied by * are significant at the 1% significance level.

small linear role in the CNN forecast, though some of these are statistically significant. The regression-based approximation to the true non-linear CNN construction explains roughly 20% to 35% of the variation in image-based predictions. But CNN predictions are built only and entirely from this raw market data. Therefore, more than half of the variation in image-based predictions is attributable to non-linear functions of the underlying market data.

Next, we use the linear specification to directly forecast returns with the approach used in Table 14. Regressions are grouped by supervising return window (5, 20, or 60 days). As a

frame of reference, columns (4), (7), and (10) report return predictive regressions using only the out-of-sample CNN forecast. Next, columns (5), (8), and (11) show another approach to linearly approximating the CNN by directly predicting returns using image-scaled market series. We find that the largest regression coefficients tend to be on the first lag of the high, low, and close prices. Together, their coefficients suggest a signal that is roughly equal to $\frac{1}{2}$(High+Low)−Close for the previous day. In other words, future returns tend to be high when the price closes at the low end of the recent high-low range. The regression also isolates features that look like deviations of the lagged prices from their recent averages. Recent rises in volume are also a notable predictor of positive future returns. These patterns are consistent with the coefficient estimates from columns (1) through (3), indicating that the CNN extracts similar patterns to those isolated by the linear model. Though, again, the linear pattern explains less than half of the content in CNN predictions.

How differentiated, and how useful, are the CNN's non-linear predictions compared to a linear model? Columns (6), (9), and (12) answer this by regressing of realized returns on CNN predictions while controlling for the image-scaled market data. First, we see that controlling for the underlying market data slightly increases the predictive coefficient on the CNN-based forecast. The logistic regression R^2 using only the CNN as a predictor ranges from 0.9% to 1.6%. The linear approximation delivers an R^2 of 0.5% to 1.0%, and the combined R^2 in the third column of each group of regressions is nearly the same as the CNN-only regression. This indicates that the non-linear component of the CNN forecast incorporates useful additional information from the underlying images relative to the linear model.

Table 16 compares the performance of long-short decile spread portfolios formed on CNN forecasts versus the regression-based linear approximation. This is reported in the rows labeled "Linear (image scale)". It shows that the linear approximation to the CNN delivers a successful trading strategy, but is generally inferior to the full non-linear CNN model (and generally superior to the benchmark models reported earlier). The linear approximation is most competitive at longer horizons, where the linear 60-day holding period strategies in some cases outperform the full CNN.

The strength of trading strategies based on the linear model begs the question: is the image representation necessary at all? Or would a linear model with a traditional time series representation of past data work just as well? To demonstrate the key role of representing market data as an image, we also study linear prediction models based on more "standard" time series representations. Of course *some* scaling choice must be made for market data to be comparable across stocks in a linear model. One obvious candidate is to scale all prices by the first closing price in the historical data window (i.e., the closing price either 5, 20, or

Table 16: Portfolio Performance of CNN versus Linear Model

	5-day Images		20-day Images		60-day Images	
	Equal Weight	Value Weight	Equal Weight	Value Weight	Equal Weight	Value Weight
			5-day Return Horizon			
CNN	7.15	1.49	6.75	1.74	4.89	1.44
Linear (image scale)	5.56	1.60	4.82	1.52	4.91	1.83
Linear (return scale)	2.50	0.23	1.19	0.36	1.14	0.46
CNN1D (image scale)	7.20	1.66	7.88	1.84	7.85	2.61
CNN1D (return scale)	5.33	1.71	5.36	1.52	5.45	1.85
			20-day Return Horizon			
CNN	2.35	0.45	2.16	0.49	1.29	0.17
Linear (image scale)	2.07	0.66	1.99	0.44	1.23	0.34
Linear (return scale)	0.51	0.11	0.41	0.33	0.43	0.30
CNN1D (image scale)	2.49	0.70	2.72	0.59	2.45	0.88
CNN1D (return scale)	1.47	0.67	1.45	0.57	1.46	0.44
			60-day Return Horizon			
CNN	1.30	0.47	0.37	0.32	0.43	0.23
Linear (image scale)	1.19	0.54	0.75	0.43	0.74	0.63
Linear (return scale)	-0.04	-0.07	0.07	0.19	0.13	0.17
CNN1D (image scale)	1.28	0.48	1.04	0.44	0.76	0.49
CNN1D (return scale)	0.24	0.19	0.35	0.21	0.24	-0.06

Note: The table reports annualized Sharpe ratios of long-short decile spread portfolios (with equal weights or value weights) sorted on out-of-sample predicted up probability from each model. "CNN" is the baseline 2D CNN, "linear" is the linear regression model, and "CNN1D" is the time series CNN model. "Return scale" indicates that market prices are normalized by the closing price at the start of each image while "image scale" indicates the high/low price normalization used to produce images.

60 days ago) and likewise for volume. We refer to this as "return scale" because prices are essentially represented as cumulative returns. The trading strategy based on a linear model with this data representation is shown in the rows "Linear (return scale)." While this model also produces positive trading performance across the board, it is substantially weaker than the linear model with image-scaled market data. For example, with 20 days of historical data, the equal weight 20-day holding period strategy drops from an annualized Sharpe ratio of 2.0 in the "Linear (image scale)" case to 0.4 for "Linear (return scale)." For value weight strategies, "Linear (return scale)" is again worse than "Linear (image scale)" for all the nine cases.

Cumulative return scaling continues to look at prices in levels. In unreported analysis, we use another representation return that converts prices into daily returns; i.e., features are converted from levels to changes. Given the standard asset pricing approach of building price trend signals from past returns, this is perhaps the most natural data representation for a linear model. But the trading strategy performance from the daily returns representation is inferior to of the price level representations (and is omitted from the table). As an example,

the I20R20 linear model using daily returns and daily volume changes produces a decile spread Sharpe ratio of 0.42 and 0.30 for equal and value weight strategies.

As a last point of emphasis for the importance of the image representation, we analyze 1D CNN models. These are time series CNN models in the sense that they use a continuous numerical representation of market data time series, and perform convolution only by sliding convolutional filters along the time series dimension of the data matrix. "CNN1D (image scale)" reports a trading strategy when the 1D CNN is applied to market data time series with image scaling, and "CNN1D (return scale)" shows the case with data normalized by initial closing price and volume. Two interesting points emerge. The first is that with image scaling, the 1D CNN performs roughly as well as, and in some cases better than, the baseline 2D CNN model. This, however, is not because the 1D CNN is superior to the 2D CNN for return prediction more generally. We see that "CNN1D (return scale)" broadly underperforms the baseline 2D CNN, as well as underperforming the "CNN1D (image scale)" model. In other words, the key performance differentiator, be it for a 2D CNN, a 1D CNN, or a linear model, is using an image representation. Once the data is represented as an image, either literally (as in our baseline case) or figuratively (using image scaling of time series data), a deep learning model can use historical market data to produce powerful return forecasts.

6.3 Visualizing the Model

The machine learning literature has long searched for methods to aid interpretation of deep learning models. Our third approach for interpreting our estimated CNNs uses a visualization technique from the machine learning literature known as gradient-weighted class activation mapping, or "grad-CAM" (Selvaraju et al., 2017). For each class ("up" or "down" returns in our setting), Grad-CAM produces heatmaps for each layer of the CNN that illustrate the regions of the input most important for predicting a class. When plotted for individual observations, these activation heatmaps help describe which aspects of the image are the most important determinants of the CNN's prediction.

In the interest of space, we focus our illustration on one variant of our CNN, the I20R20 model. We randomly draw ten images from the last year of our sample (2019) that the CNN classified as "up," and ten images it classified as down. Figure 13 shows the original image and the grad-CAM heatmap at each of the CNN's four layers. For both "up" and "down" examples, the CNN is most intensively activated amid high volatility—i.e., when the high-low range is wide. In the second and third layers, we see that the model pays special attention to open and close prices, with these appearing as especially bright points. We see further that, in the fourth layer, higher volume days accentuate the brightness of the price series. The volume region itself is only activated in the fourth layer on days with especially high volume, in

Figure 13: I20R20 Grad-CAM for 20 Images from 2019

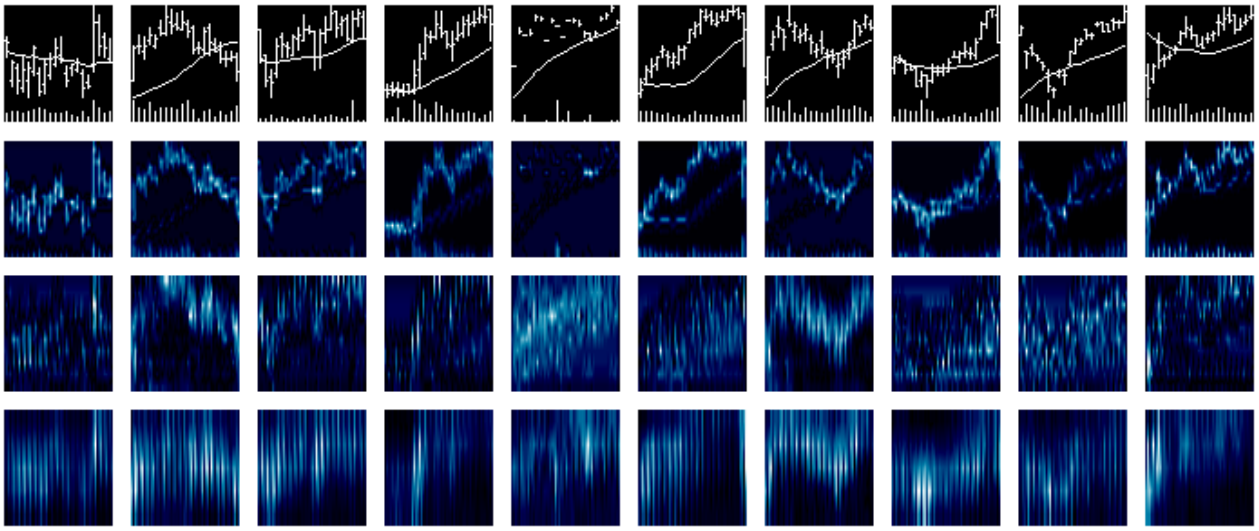

(a) Images Receiving "Up" Classification

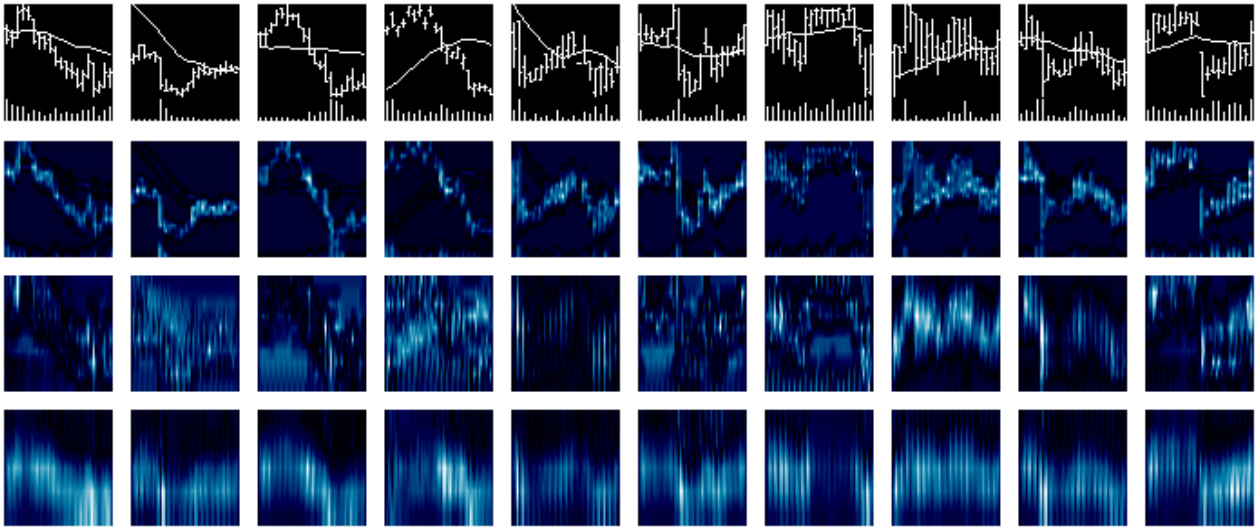

(b) Images Receiving "Down" Classification

Note: Brighter regions of the heatmap correspond to regions with the higher activation. For each panel, the first row is the original images followed by the grad-CAM for each layer in the CNN.

which case the volume bars blend together with the price bars to form wide vertical activation regions. We also see that "up" examples show especially high activation in the upper regions of the image and "down" examples are most heavily activated in the bottom half of the image.

The machine learning literature continues to grapple with interpretation of highly predictive yet complex models, and our model is an example of the interpretation challenges that deep learning faces. Nonetheless, the grad-CAM visualization helps illustrate the complicated

non-linear associations between price, high-low range, and volume that together translate into successful return prediction.

7 Conclusion

We encode market data as images and analyze them with a return prediction CNN. The CNN constructs image-based forecasts that in general outperform (and are largely distinct from) traditional price trend signals in the asset pricing literature. We show that the predictive patterns isolated by the CNN are highly robust to variations in model specification and controlling for a wide range of alternative predictor variables. One of the most compelling aspects of CNN robustness is its transferability to other time scales and international markets. Models trained on daily data are similarly powerful when transferred to data sets sampled at lower frequencies, and models trained on US data but applied to international stock markets outperform models trained on data from local markets.

In a sprawling survey of 692 asset managers in five countries, Menkhoff (2010) finds that 87% of those surveyed rely on some form of technical analysis in their process, and 18% of respondents indicate it is a major part of their investment process. As the Lo et al. (2000) at the start of this article notes, technical analysis is a primarily visual mode of analysis. In light of this, our CNN model has potentially intriguing implications for economic modeling. If trading decisions implied by a statistical representation benefit from being more closely aligned with the formats in which investors intake their market perceptions for eventual trading decisions, the CNN becomes more than a pure statistical tool and moves closer to a model of investor perception. Our ideal research agenda is to develop a model that can translate visual data into an optimal portfolio in a way that mimics the human perceptions and decision processes. In this paper, we take a first modest step in this direction by extracting trading signals from price images using a CNN model.

Market data images, when combined with a CNN, constitute a new and powerful tool for understanding market dynamics and forming efficient portfolios. Yet the images that we generate and analyze are by any measure rudimentary. In light of this, our findings highlight image analysis as a future research direction with great potential to improve our understanding of financial market phenomena.

References

Bajgrowicz, Pierre, and Olivier Scaillet, 2012, Technical trading revisited: False discoveries, persistence tests, and transaction costs, *Journal of Financial Economics* 106, 473–491.

Barberis, Nicholas, Andrei Shleifer, and Robert Vishny, 1998, A model of investor sentiment, *Journal of financial economics* 49, 307–343.

Blume, Lawrence, David Easley, and Maureen O'hara, 1994, Market statistics and technical analysis: The role of volume, *The Journal of Finance* 49, 153–181.

Brock, William, Josef Lakonishok, and Blake LeBaron, 1992, Simple technical trading rules and the stochastic properties of stock returns, *The Journal of finance* 47, 1731–1764.

Brown, David P, and Robert H Jennings, 1989, On technical analysis, *The Review of Financial Studies* 2, 527–551.

Campbell, John Y, and Samuel B Thompson, 2008, Predicting excess stock returns out of sample: Can anything beat the historical average?, *The Review of Financial Studies* 21, 1509–1531.

Chen, Jou-Fan, Wei-Lun Chen, Chun-Ping Huang, Szu-Hao Huang, and An-Pin Chen, 2016, Financial time-series data analysis using deep convolutional neural networks, in *2016 7th International conference on cloud computing and big data (CCBD)*, 87–92, IEEE.

Cont, Rama, 2005, Long range dependence in financial markets, in *Fractals in engineering*, 159–179 (Springer).

Dalal, Navneet, and Bill Triggs, 2005, Histograms of oriented gradients for human detection, in *2005 IEEE computer society conference on computer vision and pattern recognition (CVPR'05)*, volume 1, 886–893, IEEE.

Detzel, Andrew, Hong Liu, Jack Strauss, Guofu Zhou, and Yingzi Zhu, 2020, Learning and predictability via technical analysis: Evidence from bitcoin and stocks with hard-to-value fundamentals, *Financial Management* .

Dobrev, Dobrislav, 2007, Capturing volatility from large price moves: generalized range theory and applications, *Manuscript, Department of Finance, Kellogg School, Northwestern University* .

Fama, Eugene F, and Kenneth R French, 1988, Dividend yields and expected stock returns, *Journal of financial economics* 22, 3–25.

Freund, Yoav, and Robert E Schapire, 1995, A desicion-theoretic generalization of on-line learning and an application to boosting, in *European conference on computational learning theory*, 23–37, Springer.

Glorot, Xavier, and Yoshua Bengio, 2010, Understanding the difficulty of training deep feedforward neural networks, in *Proceedings of the thirteenth international conference on artificial intelligence and statistics*, 249–256.

Goodfellow, Ian, Yoshua Bengio, and Aaron Courville, 2016, *Deep learning* (MIT press).

Grundy, Bruce D, and Maureen McNichols, 1989, Trade and the revelation of information through prices and direct disclosure, *The Review of Financial Studies* 2, 495–526.

Gu, Shihao, Bryan Kelly, and Dacheng Xiu, 2020, Empirical asset pricing via machine learning, *Review of Financial Studies* 33, 2223–2273.

Han, Yufeng, Guofu Zhou, and Yingzi Zhu, 2016, A trend factor: Any economic gains from using information over investment horizons?, *Journal of Financial Economics* 122, 352–375.

Hoseinzade, Ehsan, and Saman Haratizadeh, 2019, Cnnpred: Cnn-based stock market prediction using a diverse set of variables, *Expert Systems with Applications* 129, 273–285.

Hu, Guosheng, Yuxin Hu, Kai Yang, Zehao Yu, Flood Sung, Zhihong Zhang, Fei Xie, Jianguo Liu, Neil Robertson, Timpathy Hospedales, et al., 2018, Deep stock representation learning: From candlestick charts to investment decisions, in *2018 IEEE international conference on acoustics, speech and signal processing (ICASSP)*, 2706–2710, IEEE.

Ioffe, Sergey, and Christian Szegedy, 2015, Batch normalization: Accelerating deep network training by reducing internal covariate shift, *arXiv preprint arXiv:1502.03167* .

Jegadeesh, Narasimhan, and Sheridan Titman, 1993, Returns to buying winners and selling losers: Implications for stock market efficiency, *The Journal of finance* 48, 65–91.

Kelly, Bryan, and Seth Pruitt, 2013, Market expectations in the cross-section of present values, *The Journal of Finance* 68, 1721–1756.

Kim, Taewook, and Ha Young Kim, 2019, Forecasting stock prices with a feature fusion lstm-cnn model using different representations of the same data, *PloS one* 14, e0212320.

Kinga, D, and J Ba Adam, 2015, A method for stochastic optimization, in *International Conference on Learning Representations (ICLR)*, volume 5.

Lee, Jinho, Raehyun Kim, Yookyung Koh, and Jaewoo Kang, 2019, Global stock market prediction based on stock chart images using deep q-network, *IEEE Access* 7, 167260–167277.

Lo, Andrew W, and Jasmina Hasanhodzic, 2010, *The heretics of finance: Conversations with leading practitioners of technical analysis*, volume 16 (John Wiley and Sons).

Lo, Andrew W, Harry Mamaysky, and Jiang Wang, 2000, Foundations of technical analysis: Computational algorithms, statistical inference, and empirical implementation, *The journal of finance* 55, 1705–1765.

Maas, Andrew L, Awni Y Hannun, and Andrew Y Ng, 2013, Rectifier nonlinearities improve neural network acoustic models, in *Proc. icml*, volume 30, 3.

Mandelbrot, Benoit B, 2013, *Fractals and scaling in finance: Discontinuity, concentration, risk. Selecta volume E* (Springer Science & Business Media).

Menkhoff, Lukas, 2010, The use of technical analysis by fund managers: International evidence, *Journal of Banking & Finance* 34, 2573–2586.

Neely, Christopher J., David E. Rapack, Jun Tu, and Guofu Zhou, 2014, Forecasting the equity risk premia: The role of technical indicators, *Management Science* 60, 1772–1791.

Pan, Sinno Jialin, and Qiang Yang, 2009, A survey on transfer learning, *IEEE Transactions on knowledge and data engineering* 22, 1345–1359.

Papageorgiou, Constantine P, Michael Oren, and Tomaso Poggio, 1998, A general framework for object detection, in *Sixth International Conference on Computer Vision (IEEE Cat. No. 98CH36271)*, 555–562, IEEE.

Parkinson, Michael, 1980, The extreme value method for estimating the variance of the rate of return, *The Journal of Business* 53, 61–65.

Schwert, G. William, 2003, Chapter 15 anomalies and market efficiency, in *Financial Markets and Asset Pricing*, volume 1 of *Handbook of the Economics of Finance*, 939 – 974 (Elsevier).

Selvaraju, Ramprasaath R, Michael Cogswell, Abhishek Das, Ramakrishna Vedantam, Devi Parikh, and Dhruv Batra, 2017, Grad-cam: Visual explanations from deep networks via gradient-based localization, in *Proceedings of the IEEE international conference on computer vision*, 618–626.

Simonyan, Karen, and Andrew Zisserman, 2015, Very deep convolutional networks for large-scale image recognition, in *ICLR*.

Srivastava, Nitish, Geoffrey Hinton, Alex Krizhevsky, Ilya Sutskever, and Ruslan Salakhutdinov, 2014, Dropout: A Simple Way to Prevent Neural Networks from Overfitting, *The Journal of Machine Learning Research* 15, 1929–1958.

Sullivan, Ryan, Allan Timmermann, and Halbert White, 1999, Data-snooping, technical trading rule performance, and the bootstrap, *The journal of Finance* 54, 1647–1691.

Viola, Paul, and Michael Jones, 2001, Rapid object detection using a boosted cascade of simple features, in *Proceedings of the 2001 IEEE computer society conference on computer vision and pattern recognition. CVPR 2001*, volume 1, I–I, IEEE.

Zeiler, Matthew D, and Rob Fergus, 2014, Visualizing and understanding convolutional networks, in *European conference on computer vision*, 818–833, Springer.

Zhu, Yingzi, and Guofu Zhou, 2009, Technical analysis: An asset allocation perspective on the use of moving averages, *Journal of Financial Economics* 92, 519–544.

Internet Appendix

A Classification Accuracy and Sharpe Ratio

A frequently referenced result of Campbell and Thompson (2008) maps predictive regression R^2 to Sharpe ratio gains for market timing strategies. This mapping is motivated by the fact that "R^2 statistics are small in magnitude. This raises the important question of whether they are economically meaningful."

The same question applies to classification accuracy statistics reported in Section 4.2. In this section, we illustrate the mapping from gains in classification accuracy to improvements in timing strategy Sharpe ratios, in analogy with R^2 result of Campbell and Thompson (2008).

We assume that in each period t, data for returns r_t and a predictive classifier x_t are drawn from a bivariate normal distribution

$$(r_t, x_t)' \sim \mathcal{N}(\mu, \Sigma)$$

where

$$\mu = (0,0)', \text{ and } \Sigma = \begin{pmatrix} 1 & \rho \\ \rho & 1 \end{pmatrix}.$$

That the variables are individually standard normal is without loss of generality as location and scale shifts cancel out in the portfolio analysis. We define the classifier such that $x > 0$ indicates a positive return prediction.

Population accuracy corresponds to

$$Acc(\rho) = \mathrm{E}[1_{r>0}1_{x>0} + 1_{r\leq 0}1_{x\leq 0}] = \Phi[(0,0)';\rho] + \tilde{\Phi}[(0,0)';\rho]$$

where Φ and $\tilde{\Phi}$ are the cumulative and counter-cumulative distribution functions for the bivariate normal.

In parallel, consider a trading strategy that invests $+1$ units in the asset when the classifier signals a positive return and -1 otherwise (zero forecasts can be allocated to either long or short trades since a zero has no probability mass in this example). The population Sharpe ratio of this strategy is

$$Acc(\rho) = \mathrm{E}[r1_{x>0} - r1_{x\leq 0}]/\sigma(r1_{x>0} - r1_{x\leq 0})$$

which is unaffected by the scale of r and x and depends only on their correlation.

Mapping between $Acc(\rho)$ and $SR(\rho)$ works as follows. For any given level of accuracy, a, solve for $\rho(a) = Acc^{-1}(a)$, and evaluate the Sharpe ratio at this inferred level of correlation.

Figure 14: Classification Accuracy and Sharpe Ratio

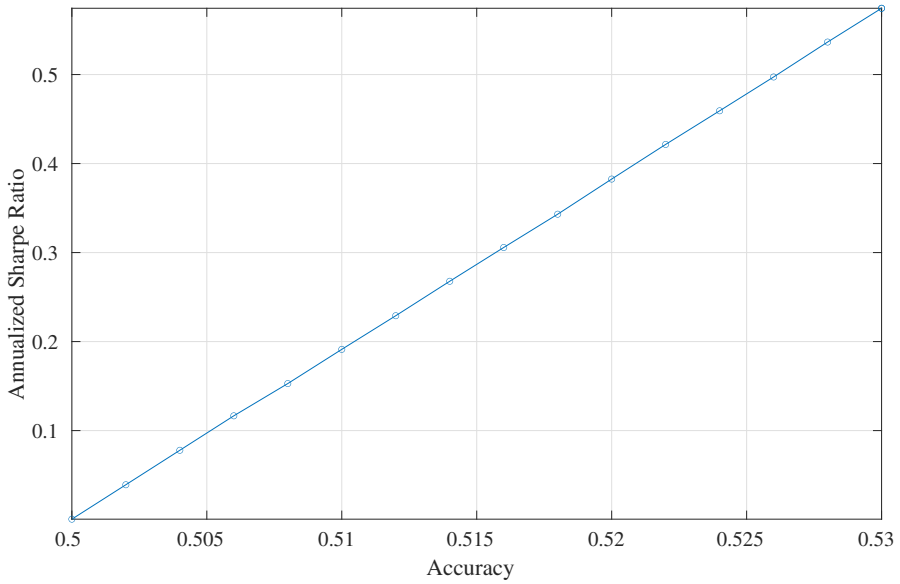

Note: The figure shows the mapping from 20-day return classification accuracy to market timing annualized Sharpe ratio in the bivariate normal example.

Finally, we must account for the frequency of observations. Intuitively, the more frequently you can bet at a given level of accuracy, the better the strategy does over a given time horizon. Defining K to be the number of periods per year, the annualized Sharpe ratio as a function of accuracy is then

$$\sqrt{K}SR(Acc^{-1}(a)).$$

Figure 14 plots this function using a range of accuracies suggested by the Table 2 estimates for 20-day returns (corresponding to $K = 12$). The figure indicates that for monthly signals, every 0.5% increase in accuracy translates into a 0.1 increase in annualized Sharpe ratio.

The derivation in this stylized example show how seemingly small gains in classification accuracy translate into large improvements in trading strategy performance.

B Robustness

B.1 Sensitivity to Data Choices, Model Structure, and Estimation Methods

In this section we conduct a number of sensitivity analyses. We report classification accuracy and annualized Sharpe ratios for long-short decile strategies (using equal and value weights). We focus on the 20-day return horizon and use images of 5, 20, and 60 days. In all sensitivity analyses, the baseline version of each variation is listed first and shown in bold.

First, in Table 17, we consider how model performance is affected by excluding volume

Table 17: Sensitivity to Data Augmentation

		I5R20			I20R20			I60R20		
			Sharpe Ratio			Sharpe Ratio			Sharpe Ratio	
		Acc.	EW	VW	Acc.	EW	VW	Acc.	EW	VW
Baseline		**0.513**	**2.35**	**0.45**	**0.525**	**2.16**	**0.49**	**0.530**	**1.29**	**0.17**
VB/MA	no VB, MA	0.506	2.42	0.55	0.509	1.03	-0.03	0.502	0.79	0.13
	VB, no MA	0.515	2.52	0.79	0.517	1.72	0.40	0.528	1.06	0.09
	no VB, no MA	0.506	2.51	0.64	0.499	0.99	0.23	0.511	0.67	0.17
Return Filter	10%	0.521	2.49	0.57	0.526	1.99	0.24	0.533	1.18	0.23
	20%	0.524	2.29	0.56	0.532	1.55	0.02	0.534	1.25	0.21
	30%	0.529	2.32	0.61	0.538	1.62	0.27	0.535	0.91	0.14
	40%	0.540	2.17	0.72	0.544	1.23	-0.02	0.547	0.77	0.26
	50%	0.549	1.94	0.46	0.551	1.25	-0.01	0.546	0.85	0.11
Largest Stocks	4000	0.536	1.67	0.52	0.526	0.85	0.35	0.524	0.21	0.16
for Training	2000	0.546	1.16	0.64	0.537	0.44	0.42	0.529	-0.10	-0.13

Note: This table reports model performance sensitivity to data variations. "VB/MA" reports the effect of excluding volume bars and/or the moving average price curve from images. "Return Filter" reports the effect of excluding x% of return with the smallest volatility-scaled returns in the training samples. "Largest Stocks for Training" reports the effect of training using only the top 4,000 or 2,000 firms in a training sample. The baseline version is listed first and shown in bold; it includes both VB and MA, uses a return filter of 0%, and uses all stocks with no size cutoff. We report classification accuracy and annualized Sharpe ratios for long-short decile strategies (using equal and value weights). Models are based on a 20-day return horizon and use images of 5, 20, and 60 days.

bars (VB) or moving average price curve (MA) from images. We report classification accuracy and annualized Sharpe ratios for long-short decile strategies (using equal and value weights). We focus on the 20-day return horizon and use images of 5, 20, and 60 days. We find that for small images (5 days), there is some gain (especially in value weight strategies) to omitting volume and moving average price. For 20-day and 60-day images, however, excluding volume and moving average information is detrimental to model performance. A possible reason for that is moving average lines create more noise than information in 5-day images, but this is not an issue for 20 and 60-day images.

In some applications, removing observations that are close to the classification boundary (i.e., returns near zero in our case) helps to de-noise the training data and improve out-of-sample performance. We consider filtering the training data to remove observations that have small returns relative to their volatility. In particular, we look at estimation variants that remove the smallest 10%, 20%, 30%, 40%, or 50% of volatility-scaled returns from the training sample. We find that this de-noising degrades model performance in general, though for 5-day images there are small benefits to using a mild filter.

Likewise, in the spirit of de-noising in training, we explore whether there are benefits to excluding the smallest stocks from the training sample, as these tend to be less liquid, more

Table 18: Sensitivity to Model Structure and Estimation, I20R20

		Loss		Acc.		Correlation		Sharpe Ratio	
		V	T	V	T	Spearman	Pearson	EW	VW
Baseline		**0.687**	**0.690**	**0.542**	**0.533**	**0.059**	**0.034**	**2.16**	**0.49**
Filters (64)	32	0.687	0.690	0.543	0.534	0.058	0.033	2.00	0.28
	128	0.689	0.691	0.538	0.530	0.054	0.031	1.85	0.40
Layers (3)	2	0.688	0.690	0.541	0.534	0.054	0.030	1.77	0.33
	4	0.688	0.691	0.541	0.531	0.052	0.031	2.14	0.22
Dropout (0.50)	0.00	0.697	0.693	0.532	0.528	0.047	0.027	2.14	0.59
	0.25	0.689	0.692	0.541	0.528	0.055	0.032	2.31	0.51
	0.75	0.688	0.691	0.540	0.530	0.053	0.030	1.47	0.16
BN (yes)	no	0.685	0.691	0.550	0.532	0.062	0.037	2.33	0.51
Xavier (yes)	no	0.688	0.692	0.541	0.527	0.056	0.032	2.08	0.44
Activation (LReLU)	ReLU	0.688	0.691	0.540	0.531	0.053	0.029	1.49	0.23
Max-pool Size (2×1)	(2×2)	0.689	0.691	0.536	0.531	0.053	0.029	1.62	0.32
FilterSize (5×3)	(3×3)	0.690	0.691	0.536	0.530	0.051	0.027	1.53	0.16
	(7×3)	0.689	0.691	0.537	0.531	0.053	0.030	1.84	0.09
Dilation/Stride (2,1)/(3,1)	(2,1)/(1,1)	0.692	0.692	0.533	0.523	0.047	0.028	2.20	0.26
	(1,1)/(3,1)	0.689	0.691	0.540	0.532	0.057	0.032	2.00	0.30
	(1,1)/(1,1)	0.693	0.693	0.534	0.521	0.051	0.029	1.80	0.25

Note: This table reports model performance sensitivity to model and estimation variations including the number of filters in the first layer (equal to 64 in baseline model), number of convolutional layers (baseline 3), dropout probability (baseline 0.50), use of batch normalization (BN, baseline yes), use Xavier initialization (baseline yes), activation function (baseline leaky ReLU), size of max-pooling layers (baseline (2,1)), filter size (baseline 5×3 pixels), and combinations of dilation and stride (baseline (2,1) and (3,1)). The columns show cross-entropy loss and prediction accuracy on the validation set (V) and the out-of-sample test set (T), out-of-sample Spearman and Pearson correlations, and annualized decile spread Sharpe Ratio with equal and value weights.

volatile, and heavier tailed. Across the board we find no benefits in model performance to limiting stocks to the top 4,000 or top 2,000 stocks during training.

In Table 18, we explore performance sensitivity to various dimensions of model structure and estimation choices. We report sensitivity in terms of loss function value, classification accuracy, average cross-sectional correlation of forecasts with return realizations (both Pearson and Spearman rank correlation), and annualized Sharpe ratios for long-short decile strategies. For loss and accuracy, we report statistics for both the validation (V) and test (T) samples. Correlations and Sharpe ratios are for the test sample only.

First, we report the effect of varying the number of filters in the first layer of the CNN from 64 down to 32 or up to 128. We see that model performance is fairly insensitive to the number of filters. Next, we increase/decrease the number of convolution layers from 3 to 2 or 4. Decreasing the number of filters meaningfully reduces the performance of the model in terms of predictive correlations and trading performance (but has little detectable effect on

Figure 15: HAAR-like Features

Note: This figure shows the five types of HAAR-like features. Each type corresponds to a feature calculated by taking the differences between the sum of pixels over red and green regions.

loss and accuracy). The model is essentially unchanged if we lower the dropout probability, though raising it to 0.75 produces a noticeable loss in performance. Performance is insensitive to omitting the batch normalization step or Xavier initialization, but we see a loss in trading strategy performance when we transition from leaky ReLU to ReLU. Changing the max-pooling size from (2×1) to (2×2) reduces the performance significantly. Either smaller filters or larger filters hurt performance. Finally, we notice some loss in performance when we alter dilation, though the results in this dimension are mixed.

Overall, the broad conclusion of this analysis is that our main results are robust to alternative modeling choices.

B.2 Comparison With Other Computer Vision Models

In this subsection, we compare CNN to two classical visual recognition methods, namely, Adaboost with HAAR-like Features by Viola and Jones (2001) and Histogram of Oriented Gradients (HOG) by Dalal and Triggs (2005), both of which are widely used precursors to CNN. A distinction between CNN and these methods is that CNN need little or no data pre-processing and automatically extract features from the data, while features in the precursor algorithms are hand-engineered. Indeed, neither method works directly with raw pixel images at all; instead they rely on pre-selected features extracted from the pixels, in contrast to CNN.

B.2.1 Adaboost with HAAR-like Features

HAAR-like features are first introduced in Papageorgiou et al. (1998), which later gained popularity due to its widely adopted applications in real-time face detection proposed by Viola and Jones (2001). The HAAR-like features are reminiscent of HAAR basis functions in rectangle shapes, which manage to capture the differences in intensity within a region of image. For example, when used for face detection, it is shown in Viola and Jones (2001) that certain HAAR-like features learn that the region of eyes is darker than the region of the nose and cheeks.

There are five types of rectangles, as illustrated in Figure 15, colored in red and green, respectively. A feature is constructed by taking the difference between the total sums of the

pixels from two colored rectangular regions of a detection window. Because the detection window slides over the entire image and its size can vary arbitrarily within the image, the total number of features constructed is massive. Specifically, there are over 100K features for a 5-day image of size 32×15, 7 million for a 20-day image of size 64×60, and 140 million for a 60-day image of size 96×180. Most of these features are either useless or redundant.

To combine these features, Viola and Jones (2001) adopt a boosting algorithm, Adaboost first introduced by Freund and Schapire (1995), that incorporates an increasing number of weak learners, which in this case are individual features themselves. The final output of the algorithm is a classification probability by (weighted) voting from selected weak learners.

B.2.2 Histogram of Oriented Gradients (HOG)

Similarly, the HOG method creates features from the input image by extracting the distribution (histograms) of directions of gradients (oriented gradients) at each pixel. As coordinates of pixels in an image are discreet, the horizontal gradient of that pixel is simply defined as the color difference between the adjacent pixels on the left and right (denoted as g_x) and the vertical gradient as the color difference between the adjacent pixels on the top and bottom of it (denoted as g_y).[16] Only four neighboring pixels are need to calculate the gradient for each centered pixel whose value is not used. The magnitude of the gradient vector is given by $|g| = \sqrt{g_x^2 + g_y^2}$ and the direction by $\Theta_g = arctan(g_y/g_x)$. Intuitively, $|g_x|$ detects vertical edges, where there is substantial difference between the left and right pixels, and similarly $|g_y|$ for horizontal edges. As a result, $|g|$ detects regions of abrupt intensity changes, e.g., edges and corners, and Θ_g detects the orientations.

The resulting gradients are grouped into bins (like a histogram) and their summary statistics based on these bins are used as features. We follow the canonical approach by dividing the image into many cells of 8×8 pixels and creating a feature for each cell. An 8×8 cell has 64 values of gradient magnitude and 64 values of gradient direction. Using the histogram of gradients, these 128 values are summarized by a 9-dimensional vector.[17] The HOG algorithm therefore effectively reduces the dimension of input variables and potentially improves the model's out of sample performance. In total, there are 192 features for 5-day images, 2,464 features for 20-day images, and 12,320 features for 60-day images. If the direction is between two bins (e.g. 15 between 0 and 20), then the votes is divided proportionally to each bins (1/4

[16] The HOG algorithm also supports colored images (e.g. RGB channels) but we focus our discussion on grey-scale images here.

[17] The histogram of all pixels in each cell is based on 9 bins corresponding to angles ranging from 0 to 180. The angles range from 0 to 180 instead of 360, the gradients are called "unsigned" gradients (a gradient and the other 180 degrees opposite to it are considered the same). We follow this tradition and use unsigned gradients. For each pixel's gradient g, Θ_g determines which bins get a share of the value $|g|$. Often Θ_g falls in between two bins, sharing the votes. The resulting feature is a size 9 vector.

to 0 and 3/4 to 20). Finally, the histogram represented by the vector of size 9 is generated for each cell of pixel size 8×8. See Figure 16 for a detailed example. In the original paper, histograms are also normalized within each block consisting of 2×2 cells. We follow the same setting in our feature generating process. The total number of features is not excessive, we thus directly use these features in a logistic regression to classify the images.

Figure 16: A Detailed Procedure to Generate HOG

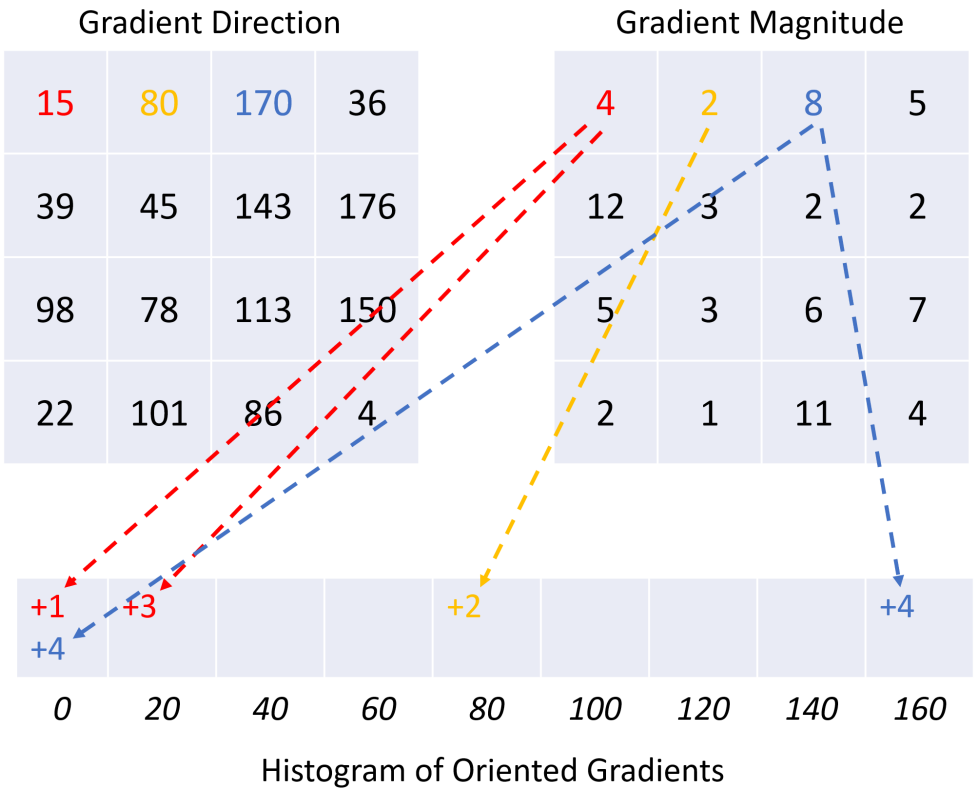

Note: For simplicity, this toy example shows the histogram from a cell of pixels size 4×4. The gradient magnitude of each pixel is divided proportionally to the bin(s) according to the gradient direction. Note that angle 170 lies between angle 160 and angle 0.

One thing to note here is that in the original HOG paper, SVM is used as the classifier. However, since we need a probability distribution of up and down moves to form the long-short portfolio, we replace SVM by logistic regression, a more intuitive classifier that directly outputs an "up" probability. In fact, we also implemented a HOG model with SVM and use the distance to the hyperplane as an alternative to up probability. The portfolio performance is inferior to the model with logistic regression. As a result, we only report the performance of HOG model with logistic regression.

To ensure a fair comparison, the same setup of our CNN model is applied to these bench-

Table 19: Comparison of Sharpe Ratios Across Computer Vision Models

Variants	CNN	HOG	HAAR	CNN	HOG	HAAR	CNN	HOG	HAAR
	I5/R5			I5/R20			I5/R60		
EW	7.15	4.11	3.62	2.35	1.59	1.26	1.30	0.58	0.34
VW	1.49	0.73	0.37	0.45	0.60	0.13	0.47	0.31	0.30
	I20/R5			I20/R20			I20/R60		
EW	6.75	2.87	2.25	2.16	0.84	0.64	0.37	0.57	0.03
VW	1.74	0.30	0.35	0.49	0.15	-0.20	0.32	0.44	0.06
	I60/R5			I60/R20			I60/R60		
EW	4.89	1.91	0.45	1.29	1.17	0.35	0.43	0.64	0.09
VW	1.44	0.36	0.46	0.17	0.19	0.30	0.23	0.11	-0.15

Note: The table compares long-short decile spread portfolio returns with equal weights (EW) and value weights (VW) based on predictions from CNN, HOG, and HAAR models.

mark models. Specifically, all models are trained with the same training dataset of CNN model. In addition, for the HOG model, 5 models are trained independently to form an ensemble model. As for the HAAR-like model, since Adaboost is already an ensemble model (with 50 weak learners), it is not necessary to apply additional ensembling.

For the HOG model, there are 192 features for 5-day images, 2,464 features for 20-day images, and 12,320 features for 60-day images. Due to the large size of the training data, the model is trained with stochastic gradient descent that minimize the log loss, which gives logistic regression. L2 norm is used as regularizer with optimal coefficient selected from 0.001, 0.0001, and 0.00001. Finally, 2/7 of the training data are set aside to be used for early stopping that stop the training process after 2 epochs without loss decreasing.

As for the model on HAAR-like features, recall that there are $142,654,368$ HAAR-like features in a 60-day image of size 96×180. It is impossible to enumerate all those features and use them for training. Due to limitation in time and computing power, we have to use a heuristic method to generate most important HAAR-like features. One popular approach to select top HAAR-like features is to train an Adaboost model on only part of training data and select features with the highest feature importance. Since the pixel images are very sparse, to further speed up the process, we also resize the images to smaller sizes before extracting features. We keep the size 32×15 of 5-day images but shrinks the size of 20-day images from 64×60 to 22×22, and the size of 60-day images from 96×180 to 16×30. After the resizing, the total number of HAAR-like features are 112392, 114433, and 112606 for 5/20/60-day images respectively. For each model, we randomly sample 10k images and train an Adaboost model on all features and select the top 100 features with the highest feature importance. Then we generate the above 100 top features for all images and train an Adaboost model with 50 weak

learners (decision stumps).

Table 19 compares the performance of decile H-L portfolios from CNN, HAAR, and HOG models. In general, CNN outperforms both HOG and HAAR with few exceptions of strategies for longer horizons.

C Monte Carlo Simulations

This section conducts simulation experiments to investigate the finite sample performance of the CNN classifier.

C.1 Simulating Images

To create images we simulate price trajectories at a 5-minute frequency, from which we obtain daily open, close, high, and low prices.

Throughout the experiments, we consider two specific patterns, Head and Shoulders Top (HNST) and Head and Shoulders Bottom (HNSB). In technical analysis, HNST is believed to indicate short-term reversal from an upward trend into a downward trend, i.e. prices are likely to drop following HNST. In the other direction, HNSB is believed to predict a future rise in prices.

The functional form for HNST is:

$$f_{hnst}(x) = \begin{cases} x, \text{ if } 0 \leq x < 1/8 \\ -x + 1/4, \text{ if } 1/8 \leq x < 1/4 \\ x - 1/4, \text{ if } 1/4 \leq x < 1/2 \\ -x + 3/4, \text{ if } 1/2 \leq x < 3/4 \\ x - 3/4, \text{ if } 3/4 \leq x < 7/8 \\ -x + 1, \text{ o/w} \end{cases}, \tag{2}$$

where $x \in [0, 1]$. The functional form of HNSB negates the sign on the right hand side of equation 2. These patterns are shown in Figure 17.

To generate price trajectories with these patterns, we simulate the logarithm of the price as a mean-reverting process over $[0, T]$:

$$r^{pattern}_{t+k\Delta} := p^{pattern}_{t+k\Delta} - p^{pattern}_{t+(k-1)\Delta} = \kappa(\bar{r}_{t+k\Delta} - p^{pattern}_{t+(k-1)\Delta})\Delta + \sigma\sqrt{\Delta}\varepsilon_{t+k\Delta}, \quad k = 0, 1, 2, \ldots, 78, \tag{3}$$

where $p^{pattern}_0 = 0$, σ is drawn from $\mathcal{U}(0.2, 0.6)$ and fixed for each image but differ across images, Δ is the sampling frequency (fixed at every 5 minutes), $\varepsilon_{t+k\Delta} \sim \mathcal{N}(0, 1)$, $\kappa = 50/T$,

Figure 17: Linear Functions of HNST and HNSB Patterns

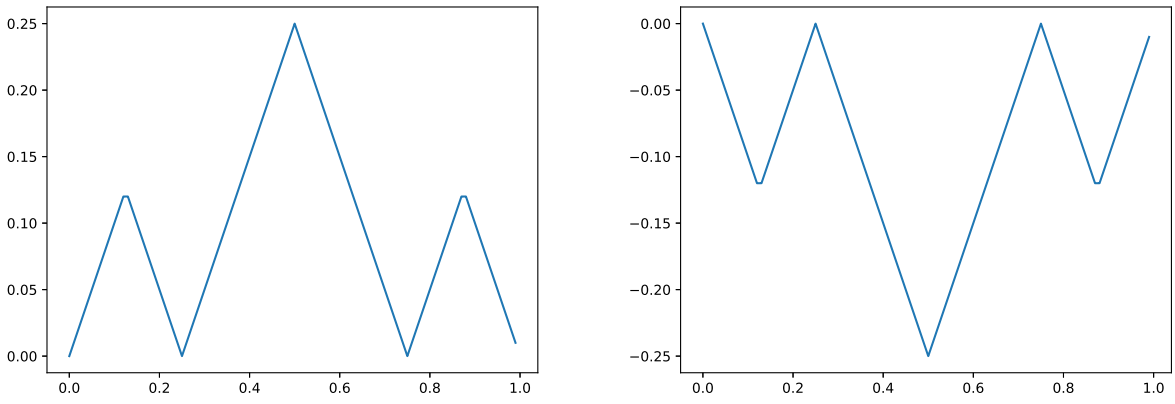

(a) HNST

(b) HNSB

$T = 20/252$ for 20-day samples (or $60/252$ for 60 days),[18] and $\bar{r}_{t+k\Delta}$ is the mean level on timestamp $t + k\Delta$ that satisfies

$$\bar{r}_{t+k\Delta} = 3\sigma\sqrt{T} f_{pattern}((t + k\Delta)/T).$$

For price trajectories without any patterns, we simply simulate a geometric Brownian motion without any drift:

$$r^{noise}_{t+k\Delta} := p^{noise}_{t+k\Delta} - p^{noise}_{t+(k-1)\Delta} = \sigma\sqrt{\Delta}\varepsilon_{t+k\Delta}, \quad k = 0, 1, 2, \ldots, 78. \tag{4}$$

Since p_t is the logarithm of price, $1 + p^{noise}_{t+k\Delta} = \sum_{s=0}^{t+k\Delta} r_s$ produces cumulative returns that appear in the image. See Figure 18 for examples of 20-day and 60-day images with and without HNS patterns.

C.2 Experiment Results

Return prediction is a rather challenging problem because the signal-to-noise ratio is notorious low. The objective of our simulations is to demonstrate how CNN models recognize patterns and make correct predictions in environments with various signal-to-noise ratios.

We start with experiments in which only one pattern (HNST or HNSB) exists in the data. We then consider experiments with both patterns included so as to check whether a CNN

[18] Because these pattern cannot be shown on a 5-day image, our simulations focus on 20-day and 60-day images.

Figure 18: Examples of Simulated Images

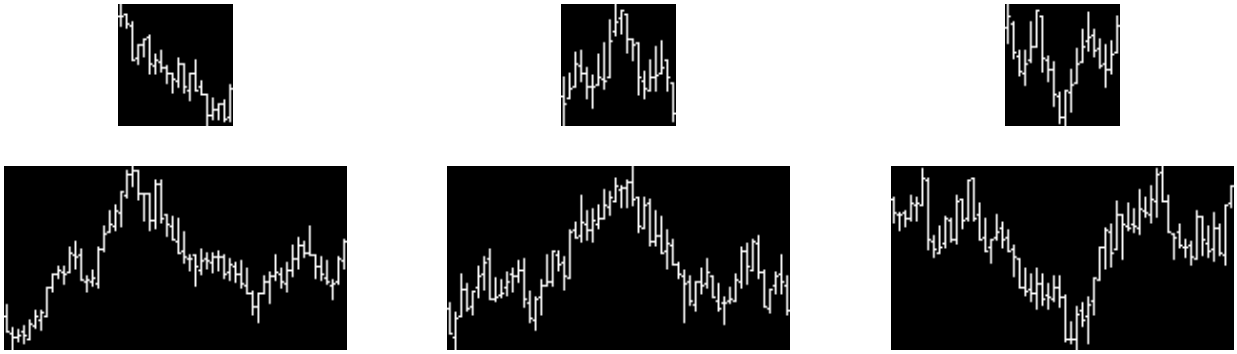

(a) Pure Noise Image (b) An HNST Image (c) An HNSB Image

Note: For each subfigure, at the top is the simulated image for 20 days and at the bottom is for 60 days.

model can recognize multiple co-existing patterns.

We conduct 100 independent experiments. In each experiment, we generate 10,000 patterned images. In the case both HNSB and HNST are included in the data, each group has 5,000 images. We then generate many more noise images such that the proportion reaches a pre-determined amount, e.g., 99.0%. We then assign "up" labels for HNST images, "down" for HNSB ones, and random "up" or "down" labels to noise images (with 50% probability). This approach controls the signal-to-noise ratio in our prediction exercise. For example, if there are 99% noise images and 1% HNST patterned images, the actual probability of an "up" move is $(99/2 + 1)\% = 50.5\%$. As the portion of noise images increases, the signal-to-noise ratio diminishes.

We maintain the same architecture design of the CNN models as in our empirical study, including 3 layers for 20-day images and 4 for 60-day ones, doubling the number of channels from bottom to top, except that we decrease the number of initial channels from 64 to 8 (and so on for subsequent layers), because our simulation setting is more stylized. The training algorithm is identical to what we use empirically, except that we increase the initial learning rate to 10^{-4} to speed up the process. Throughout all experiments, we divide all images proportionally to form the training, validation, and testing datasets, which are split according to $6 : 2 : 2$ ratios.

Figure 19 plots the average prediction accuracy on patterned images and noise images on the testing sets, respectively, against the portion of noise images in the data. We find that for both 20-day and 60-day models, the prediction accuracy is always indistinguishable from a random guess (0.5) for noise images and reaches nearly 100% on HNST and HNSB images as long as the portion of noise images drops below 99.0%, regardless of whether only a single

Figure 19: Accuracy vs Noise Ratio in Simulation

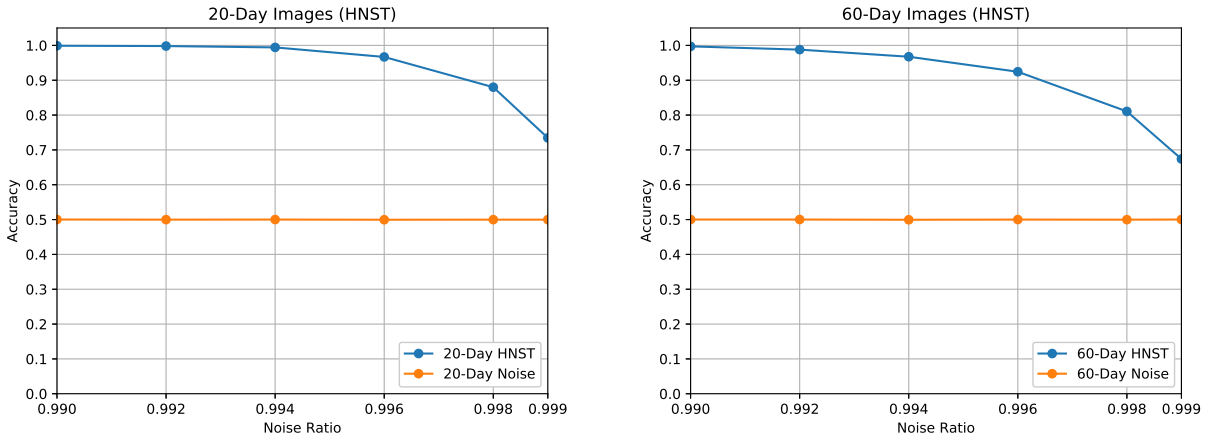

(a) Predictive accuracy for models trained with dataset that includes only HNST

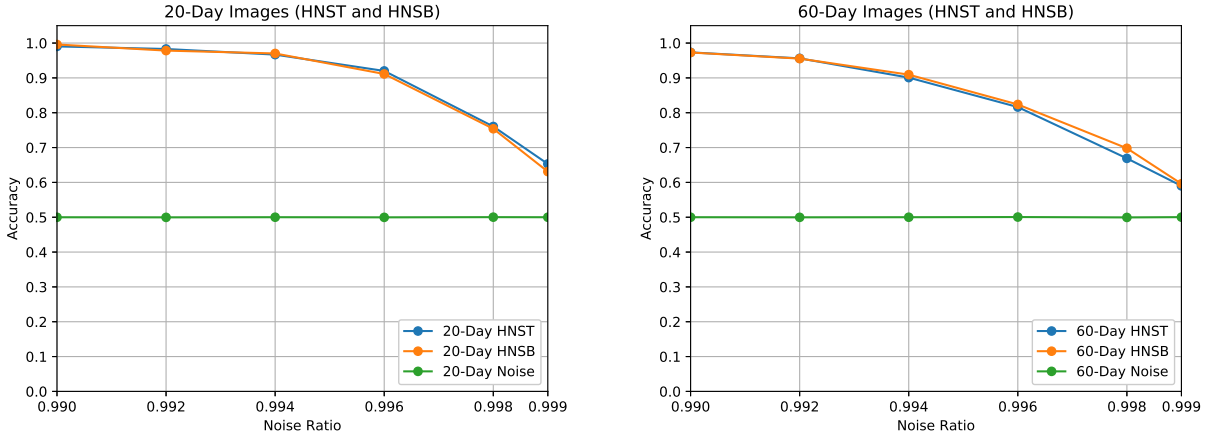

(b) Predictive accuracy for models trained with dataset that includes both HNST and HNSB

Note: For each subfigure, the left plot shows the simulation result for the 20-day model and the right plot shows that for the 60-day model. The x-axis is the noise ratio in the training set. The accuracy obtained from the OOS testing set that consists of all noise images, all HNST images, or all HNSB images. The number of Monte Carlo repetitions is 100.

pattern (top panel) or both patterns (bottom panel) are included in the datasets.

This suggests that the CNN model achieves nearly perfect recognition power on patterned images while remaining indifferent to noise ones, even though the whole dataset consists only 1% images with patterns. When only a single pattern HNST is included in the training set, with a 99.8% portion of noise images, the predictive accuracy is still as high as 0.88 for the 20-day model and 0.81 for the 60-day model. Not surprisingly, models trained with both HNST

and HNSB images (Figure 19b) perform slightly worse than models trained with HNST images alone (Figure 19a), because the number of patterned images is halved for either group.